Contrib Mineral Petrol (2006) 152: 19–42
DOI 10.1007/s00410-006-0092-5

ORIGINAL PAPER

Folco Giacomini · Rosa Maria Bomparola
Claudio Ghezzo · Hans Guldbransen

The geodynamic evolution of the Southern European Variscides: constraints from the U/Pb geochronology and geochemistry of the lower Palaeozoic magmatic-sedimentary sequences of Sardinia (Italy)

Received: 4 September 2005 / Accepted: 20 March 2006 / Published online: 22 April 2006

Abstract The high-grade metamorphic complex of northern Sardinia consists of a strongly deformed sequence of migmatitic ortho- and paragneisses interlayered with minor amphibolites preserving relic eclogite parageneses. The protolith ages and geochemical characteristics of selected gneiss samples were determined, providing new constraints for reconstructing the Palaeozoic geodynamic evolution of this sector of the Variscan chain. The orthogneisses are metaluminous to peraluminous calcalkaline granitoids with crustal Sr and Nd isotopic signatures. One orthogneiss from the high-grade zone and one metavolcanite from the volcanic belt in southern Sardinia were dated by LAM-ICPMS (and SHRIMP) zircon geochronology. The inferred emplacement ages of the two samples are 469 ± 3.7 and 464 ± 1 Ma, respectively. The analysed paragneisses are mainly metawackes with subordinate metapelites and rare metamarls. Three paragneiss samples were dated: zircon ages scatter between 3 Ga and about 320 Ma, with a first main cluster from 480 to 450 Ma, and a second one from about 650 to 550. Variscan zircon ages are rare and mostly limited to thin rims and overgrowths on older grains. These data indicate that the high-grade complex principally consists of middle Ordovician orthogneisses associated with a thick metasedimentary sequence characterised by a maximum age of deposition between 480 and 450 Ma. The association of nearly coeval felsic-mafic magmatic rocks with immature siliciclastic sedimentary sequences points to a back-arc setting in the north Gondwana margin during the Early Palaeozoic. The Variscan metamorphic evolution recorded by the high-grade gneisses (Ky-bearing felsic gneisses and mafic eclogites) testifies to the transformation of the Late Ordovician–Devonian passive continental margin into an active margin in the Devonian–Early Carboniferous.

Electronic Supplementary Material Supplementary material is available for this article at http://www.dx.doi.org/10.1007/s00410-006-0092-5 and is accessible for authorized users.

Communicated by J. Touret

F. Giacomini (✉) · R. M. Bomparola · C. Ghezzo
H. Guldbransen
Dipartimento di Scienze della Terra, Università di Siena,
via Laterina 8, 53100 Siena, Italy
E-mail: giacomini@unisi.it
Tel.: +39-0577-233802
Fax: +39-0577-233938

Introduction

An almost complete section of the southern European Variscides is well exposed in the islands of Sardinia and Corsica (Menot and Orsini 1990), where the collisional chain crops out in continuity from the almost unmetamorphosed foreland basins in southern Sardinia to the "high-grade metamorphic complex" in northern Sardinia and Corsica (Cappelli et al. 1992; Carmignani et al. 1994; Carmignani et al. 1992; Ricci 1992). The high-grade basement of northern Sardinia (Fig. 1a) is separated from the low- to medium-grade nappe zones in the south by a major mylonitic belt, the Posada-Asinara Line.

Two main geodynamic models explain the actual configuration of the southern European Variscides. A first model was originally proposed by Matte (e.g. Matte 1986; Matte 2001); it suggests that a Gondwanan promontory (indenter) collided against Armorica producing the Ibero-Armorican arc. According to several authors (among others: Cappelli et al. 1992; Carmignani and Rossi 2001; Carmignani et al. 1994; Carosi and Palmeri 2002), this collision is attested in Sardinia by the stacking of the northern high-grade metamorphic complex (an inferred pre-Cambrian Armorican fragment) over the medium to low-grade southern nappe zones (Gondwana derived). In this scenario, the presence of strongly deformed metabasites with relic eclogites along the Posada-Asinara Line is interpreted as evidence of a

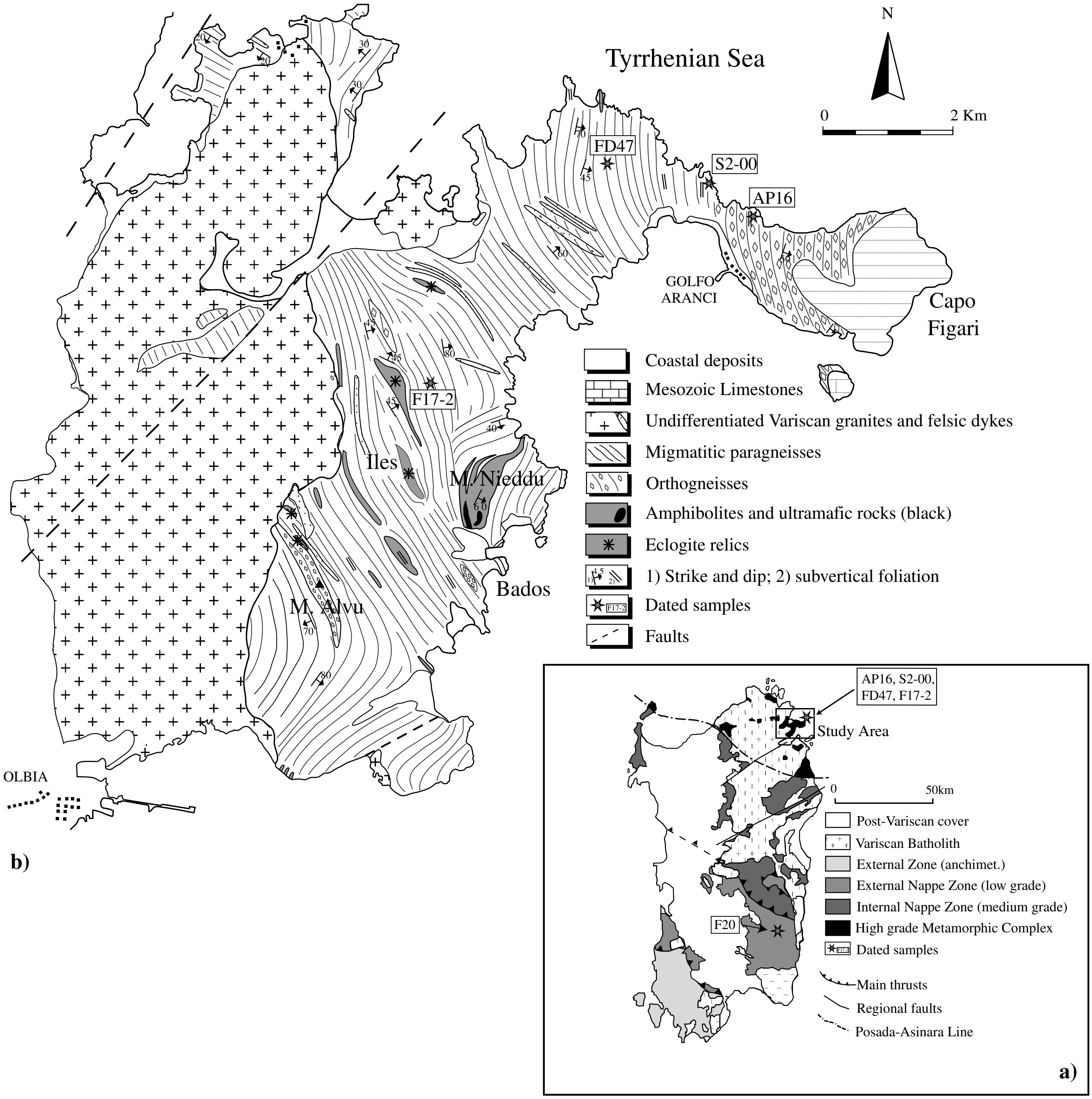

Fig. 1 **a** Simplified geological map of Sardinia island (modified after Carosi and Palmeri 2002); **b** geological map of the study area and location of dated samples

Hercynian suture zone, with the high-grade basement overriding the nappe zones.

The model proposed by Stampfli et al. (2002) and von Raumer et al. (2003) suggests alternatively that the European Variscides derive from consecutive collisions among Laurussia, the Hun Terranes—a ribbon-like assemblage of terranes detached from Gondwana starting from the Cambrian—and Gondwana itself. Following this model the whole southern European Variscides belong to the southern margin of the Hun Terranes.

Recently, structural and geochronological studies revealed striking similarities between the rocks on both sides of the Posada-Asinara Line; this led Helbing (2003) and Helbing and Tiepolo (2005) to question the presence of a suture zone between different terranes. In addition, several authors (Cortesogno et al. 2004; Palmeri et al. 2004; Giacomini et al. 2005) demonstrated the occurrence in northern Sardinia of amphibolites and eclogites originating from magmatic protoliths of the Middle Ordovician age. There is thus no general consensus about the pre-Variscan geodynamic evolution of the high-grade basement, and in most of the recently published reviews on the European Hercynian belt, the pre-Variscan position of Sardinia–Corsica, the Pyrenees and Provence is still a matter of debate (Bard 1997; Matte 1998, 2001; Edel 2000; Franke 2000; von-Raumer et al. 2003).

The aim of this work is to better constrain the geodynamic reconstructions of the pre-Hercynian history in Southern Europe, notably the tectono-magmatic evolution of the Sardinian basement, through an extensive geochemical and geochronological study of the poorly known and mostly undated felsic orthogneisses and metasediments within the high-grade Sardinian basement. In this study, in-situ U/Pb, Lu/Hf and trace element zircon compositions provided, for the first time in the region, reliable constraints for the determination of the sources and depositional ages for the strongly metamorphosed sedimentary sequences occurring in northern Sardinia.

Geological setting and petrography

According to literature, the high-grade metamorphic complex consists of felsic orthogneisses of Ordovician age (Di Simplicio et al. 1974) interlayered with dominant upper-amphibolite-facies metasediments and minor metabasites. The metabasites are characterised by Ordovician protoliths and undated eclogite-facies parageneses (Miller et al. 1976; Palmeri et al. 2004; Cortesogno et al. 2004; Giacomini et al. 2005). They occur within metasediments as concordant lenticular bodies or banded amphibolite/felsic gneiss sequences, resembling in the field the ‘‘leptynite–amphibolite complexes’’, well known in the whole European Variscides (Franceschelli et al. 2005a, and references therein). The high-grade basement is characterised by a polyphase tectono-metamorphic history with four main ductile deformation phases; peak metamorphic conditions increase northward from lower amphibolite to upper amphibolite—granulite facies (see Ricci et al. 2004, for a detailed review). The widespread occurrence of kyanite and late sillimanite ± K-feldspar, attested within a number of migmatite outcrops north of the PAL (Palmeri 1992; Cruciani et al. 2003; Giacomini et al. 2005), is ascribed to the nearly isothermal decompression at high temperature. This stage is characterised by several episodes of partial melting, leading to the development of migmatites and discordant veins of peraluminous anatectic melts. The granulite metamorphic assemblages are overprinted by lower temperature retrograde parageneses, associated with regional deformation in a transpressive dextral shear regime (Carosi and Palmeri 2002).

In the Golfo Aranci area (Fig. 1b) the basement exhibits a NW–SE trending foliation; it mainly consists of stromatic migmatites and diatexites with intercalations of felsic orthogneisses and amphibolites, which in places preserve relics of original intrusive features, despite metamorphic equilibration under eclogite-facies conditions (Franceschelli et al. 2002, 2005a; Giacomini et al. 2005). Metapelitic rocks with migmatitic fabrics are subordinate; they crop out mainly in the southernmost Golfo Aranci area (e.g. P.ta Bados). The orthogneisses are mainly monzogranitic, occasionally granodioritic or tonalitic. K-feldspar megacrysts are sometimes preserved, producing typical *augen* textures (Fig. 2a). Peraluminous granitic or aplitic dykes with different degrees of deformation pervasively intrude the orthogneiss bodies. Stromatic migmatites and diatexites (Fig. 2b) are commonly wacke to arkosic in composition. The diatexites preserve relics of former stromatic fabrics, but they are often strongly restructured, containing levels, boudins or fragments of granitic leucosomes producing agmatite-like textures. The metapelites are strongly schistose and they may contain layers of leucosome (Fig. 2c). Even though small bodies of garnet-bearing marble are reported south of the study area (e.g. Tamarispa marble, Elter and Palmeri 1992), there is no marble at Golfo Aranci. Calc-silicate rocks are limited to small boudins hosted (Fig. 2b–d) within the metapsammitic-pelitic sequences (Ghezzo et al. 1979).

Orthogneisses

The granitic gneisses (Golfo Aranci, M. Alvu) are composed of quartz, K-feldspar, plagioclase (An_{20}), subordinate biotite ($Mg/[Mg+Fe^{2+}]=0.5$) and muscovite. Apatite and small unzoned garnet grains are minor constituents; zircon and monazite are the main accessory minerals. Within the less deformed domains, plagioclase may preserve euhedral oscillatory zoning. Where deformation was stronger the *augengneisses* were transformed into mylonitic banded gneisses characterised by the alternation of quartz–feldspathic rods and mica levels. K-feldspar megacrysts were recrystallised into smaller grains intergrown with quartz; quartz grain microstructures show migrating grain boundaries and ribbon textures (Elter and Ghezzo 1995).

The granodioritic and tonalitic orthogneisses (Bados) contain plagioclase ($An_{25\text{-}35}$), biotite, quartz and hornblende as major constituents. Apatite and zircon are common accessories. White mica and K-feldspar are absent in these lithologies. Primary magmatic features are not preserved. For a detailed description of the mafic orthogneisses (amphibolites and eclogites) refer to Franceschelli et al. (2002, 2005a) and Giacomini et al. (2005).

Paragneisses ss

The best preserved migmatitic paragneisses mainly consist of quartz, plagioclase ($An_{30\text{-}44}$), biotite ($Mg/[Mg+Fe^{2+}]=0.5$) and muscovite (Si = 3.03–3.06 a.p.f.u.). Garnet (core–rim composition: $Alm_{72\text{-}68}$, $Prp_{17\text{-}12}$, $Sps_{6\text{-}15}$, $Adr_{1\text{-}3}$, $Grs_{4\text{-}2}$), K-feldspar, apatite and tourmaline may

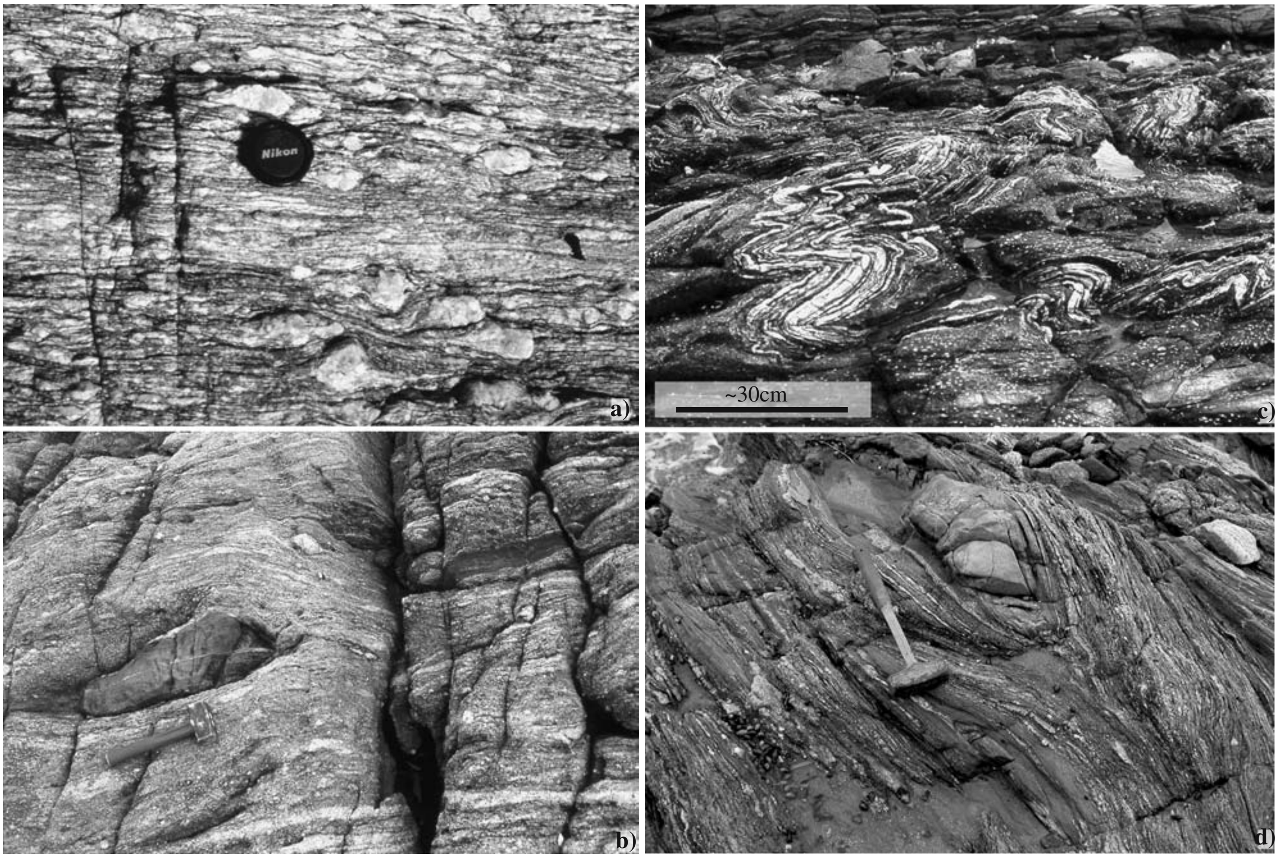

Fig. 2 **a** Monzogranitic orthogneiss with *augen* texture; **b** deformed diatexite with boudins of calc-silicate rocks and disrupted leucosome layers; **c** Ky-bearing metapelites with late Sil nodules (*white spots*) from P.ta Bados; **d** calc-silicate rock boudin embedded within typical metapelites

also occur as accessory phases. The melanosomes are composed of biotite and muscovite, with quartz, opaque minerals, apatite, zircon and monazite as accessory phases. The leucosomes are both granitic and tonalitic in composition. Plagioclase is mostly euhedral to subhedral with respect to quartz, and quartz–plagioclase myrmekites are often observed. Garnet may occur in large inclusion-rich crystals within the melanosomes or as small, subrounded crystals in the leucosomes. Rare kyanite relics are found armoured within plagioclase, whereas biotite + fibrolite selvages are sometimes found within the leucosomes.

Metapelites

Metapelites typically contain Al_2SiO_5 polymorphs in the form of kyanite porphyroblasts, sillimanite nodules or selvages. The more pelitic lithologies mainly consist of biotite, quartz, plagioclase, Al_2SiO_5 polymorphs ± garnet and rutile. Within the domains characterised by granoblastic textures, biotite has straight grain boundaries with kyanite, garnet, plagioclase and quartz. Rutile inclusions occur within kyanite porphyroblasts. Kyanite porphyroblasts are commonly rimmed by muscovite and rarely by margarite coronas. Biotite is partially replaced by tiny intergrowths of muscovite; fibrolite–muscovite or quartz–muscovite selvages overgrow the biotite foliation. K-feldspar may occur in the groundmass of the muscovite–quartz and muscovite–sillimanite selvages.

Calc-silicate rocks

The calc-silicate boudins are zoned with a dark green amphibole-rich rim and a pale rose garnet-rich core. Under the microscope the boudin rims are characterised by granular microstructures. They are mainly composed of plagioclase, quartz, clinopyroxene, garnet and titanite ± amphibole. The boudin cores consist of dominant garnet and quartz with subordinate plagioclase, clinopyroxene and titanite. Garnet (Grs_{50}) occurs in large crystal aggregates, possibly due to the coalescence of different grains during growth. The other phases generally build pseudo-granoblastic aggregates interstitial to garnet crystals, or occur as inclusions within garnet blasts.

Analytical methods

Zircon dating and chemistry

Zircon grains were concentrated using standard techniques. A Philips XL30 electron microscope equipped with a cathodoluminescence (CL) detector (Dipartimento di Scienze della Terra, Università di Siena) was used to obtain CL images of zircons. Back-scattered electron (BSE) images were collected with a CAMEBAX SX50 electron microprobe (GEMOC Key Centre, Macquarie University, Sydney). Operating conditions were an accelerating voltage of 15 kV and a beam current of 20 nA. Zircons were analysed for U, Th and Pb isotopic compositions using a 213 nm laser ablation microprobe (LAM) coupled with an Agilent 4500, series 300 ICP-MS at the GEMOC Key Centre (Macquarie University, Sydney), and a 213 nm LAM coupled with a magnetic sector ICP-MS at CNR-Istituto di Geoscienze e Georisorse of Pavia (Italy). Trace element data for the same set of zircons were collected using the same LAM-ICPMS system at CNR-Pavia. For a detailed description of the methods refer to Giacomini et al. (2005) and the references therein. U/Pb analyses of zircons from two samples were also carried out using SHRIMP at the Australian National University in Canberra. Measurement procedures are described in Compston et al. (1992).

Whole rock chemistry

Major, trace element and REE compositions of selected para- and orthogneiss samples from the Sardinian and south Corsican basement were analysed by ICP-AES spectrometry at SARM CRPG-CNRS of Nancy (France). For the analyses we selected the most homogeneous migmatitic gneisses, in order to reduce the effect of leucosome–melanosome layering on chemical composition. Sr and Nd isotopes were analysed with a VG (Micromass) Sector 54 TIMS at the Pacific Centre for Isotopic and Geochemical Research (PCIGR), Vancouver.

Geochronology

In-situ U/Pb ages of zircons

U–Pb LAM-ICPMS dating of zircon crystals was carried out on one representative orthogneiss sample (AP16) and on three different paragneiss samples representative of two stromatic migmatites (FD47, F17-2) and a diatexite (S2-00). An anchi-metamorphosed rhyodacite (F20) cropping out in the external nappe zone of southern Sardinia (sampling area: rio Leunaxi–Sarrabus, Fig. 1a) was also analysed to compare the effusive sequences of southern Sardinia and the orthogneisses of northern Sardinia. According to literature (Carmignani et al. 1992; Garbarino et al. 2005), these volcanic rocks are of Middle Ordovician age, as they are interlayered between Cambro-Ordovician metasandstones (“S. Vito Sandstones”) and Caradocian metasediments (“P.ta Serpeddì Formation”).

SHRIMP analyses were carried out on zircons from samples AP16 and S2-00 in order to compare the results obtained by means of LAM-ICPMS.

Ablation spots for geochronology were chosen so as to represent the heterogeneity of zircon structures. Efforts were made to avoid analysing areas with cracks and inclusions, and analytical spots were selected after the characterisation of zircons under transmitted light, CL and BSE images (Fig. 3). Tables 1, 2, 3 and 4 report the selected isotope and trace element compositions of analysed zircons. For the complete dataset, refer to Tables 5–13 (electronic supplementary material). *Orthogneiss AP16*. Zircons in the AP16 orthogneiss concentrate mainly within biotite grains. They are generally euhedral, short-prismatic to strongly elongated, have sharp edges and vary in dimension from a few tens to several hundred microns. In CL and BSE images, most grains show evident oscillatory growth zoning. Inherited cores are rare. U–Pb results are shown in Fig. 4a. In the Tera–Wasserburg plot, most of the data define a concordant group of zircons, with ages spanning from 497 to 431 Ma (34 analyses) in zircons analysed by LAM-ICPMS, and from 478 to 431 Ma (23 analyses) in zircons analysed by SHRIMP. In the density plot the LAM-ICPMS data define three main peaks at 474 ± 3.6 (9 analyses), 453 ± 3.3 (21 analyses) and 434 ± 4.7 Ma (4 analyses), although the range of U–Pb ages is continuous with no real gaps between the three populations. The choice of the most realistic emplacement age therefore relies on a detailed study of zircon structures. Only data on zircon domains characterised by clear igneous textures (oscillatory zoning) and lacking older inherited components, younger overgrowths and texturally complex domains were used to obtain the age of the emplacement. The best weighted average estimate for 16 analyses is 469 ± 3.7 Ma (MSWD = 1.6). The younger ages are probably related to lead loss events; their concordance is most likely due to the short time that elapsed between emplacement and the event that produced lead loss. There is also a data point at 384 ± 4.7 Ma. The SHRIMP data define a restricted range (21 of 23 analyses) of concordant ages whose weighted average age is 466 ± 3 (MSWD = 1.6). The weighted mean ages and uncertainties (given at the 95% confidence level) were calculated using LAM-ICPMS $^{207}Pb/^{206}Pb$ concordant ages and SHRIMP $^{206}Pb/^{238}U$ ages. Both techniques yielded equivalent results within analytical uncertainties: the larger spread of the LAM-ICPMS U–Pb data is due to the greater number of analyses obtained with this instrument and to the wider range of analysed zircon structures. The few inherited concordant cores (two from LAM-ICPMS, one from SHRIMP analyses) span between 665 and 575 Ma.

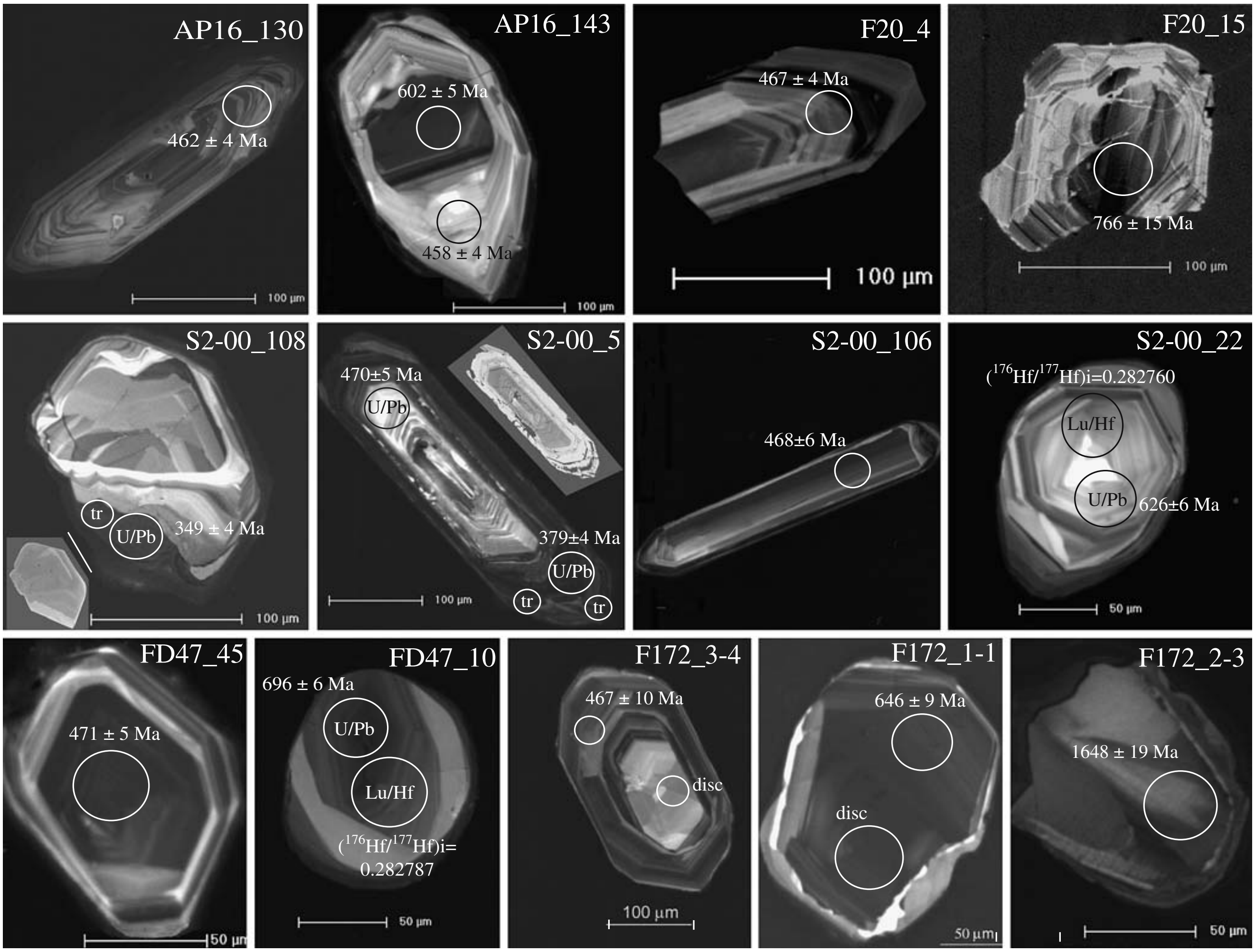

Fig. 3 CL photomicrographs of representative zircons of the dated samples with the location of analytical spots and results. The small photographs with *grey* background are BSE images of zircons showing bright metamorphic overgrowths

Metarhyodacite F20

The zircon population of sample F20 is rather heterogeneous, and zircons are often fractured. They are generally euhedral, short and prismatic, but elongated grains 50–150 µm in length are also present. Internal zoning varies from oscillatory growth zoning to convolute. Evidence for overgrowths and inherited cores is common. With the aim of dating the magmatic event related to the eruption of the volcanic protolith, we concentrated the analyses on zircons characterised by well-developed oscillatory zoning, without complex textures. A few inherited cores were also analysed. Results are not completely satisfactory: of the 19 analysed spots, one gave a discordant age and six inversely discordant ages (Fig. 4a). The remaining points range between 767 and 417 Ma, with five points defining a mean concordant age of 464 ± 1 Ma (MSWD = 1.9). The older ages were obtained for the cores of zircons showing evidence of overgrowth at the rim. The ages of 429 and 417 Ma were obtained for the rims of two zircons with cores as old as 644 and 466 Ma, respectively.

Diatexite S2-00

The zircon population of the S2-00 diatexitic paragneiss is rather heterogeneous: euhedral, short-prismatic and elongated crystals with relatively sharp edges are most common, but short-prismatic to equant subhedral and rounded grains are also present. BSE and CL images (Fig. 3) show that the internal structure of grains varies greatly. The euhedral short-prismatic and elongated grains usually have well-developed, magmatic-like oscillatory zoning and contain mineral inclusions (mainly quartz and apatite). The zoning is sometimes truncated by overgrowths that form convoluted bands or thin rims. Inherited cores with different zoning are common, but very old components are also present as unzoned subrounded whole grains. The BSE images of a few zircons from the S2-00 diatexite reveal the presence of bright patches and of strongly zoned rims with alternating brighter and darker regions: these rims, most likely affected by metamict processes, are often fractured and appear as very dark areas in the CL images.

Table 1 Selected LAM-ICPMS U-Th-Pb isotope data and calculated ages for zircons from the analysed samples (further data available as electronic supplementry material)

Analysis	Measured rations								Ages (Ma)							
	$^{207}Pb/^{206}Pb$	1σ	$^{207}Pb/^{235}U$	1σ	$^{206}Pb/^{238}U$	1σ	$^{208}Pb/^{232}Th$	1σ	$^{207}Pb/^{206}Pb$	1σ	$^{207}Pb/^{235}U$	1σ	$^{206}Pb/^{238}U$	1σ	$^{208}Pb/^{232}Th$	1σ
Orthogneiss																
AP16-130R[a]	0.05679	0.0006	0.57884	0.0074	0.07387	0.0009	0.02187	0.00034	483	23	464	5	459	6	437	7
AP16-143C[a]	0.06139	0.0007	0.81796	0.0108	0.09661	0.0013	0.02861	0.0003	653	24	607	6	595	7	570	6
AP16-143R[a]	0.05553	0.0007	0.56641	0.0085	0.07394	0.0010	0.02191	0.0005	434	29	456	6	460	6	438	10
AP16-176R[a]	0.05625	0.0008	0.57935	0.0089	0.0747	0.0009	0.02137	0.0003	462	34	464	6	464	5	427	6
AP16-185[a]	0.05924	0.0009	0.76231	0.0124	0.09327	0.0012	0.02763	0.0004	576	33	575	7	575	7	551	7
Meta-rhyodacite																
F20_4[b]	0.0562	0.0007	0.5829	0.0058	0.0752	0.0006	n.a.	n.a.	459	26	466	4	468	4	–	–
F20_6[b]	0.05643	0.0007	0.5778	0.0062	0.0743	0.0006	n.a.	n.a.	469	28	463	4	462	4	–	–
F20_9C[b]	0.06186	0.0008	0.8919	0.0108	0.1045	0.0009	n.a.	n.a.	669	29	647	6	641	5	–	–
F20_15[b]	0.06574	0.0014	1.1400	0.0236	0.1259	0.0014	n.a.	n.a.	798	44	773	11	764	8	–	–
Diatexite																
S2-00_1[a]	0.05629	0.0007	0.5818	0.0081	0.07493	0.0009	0.02382	0.0002	464	29	466	5	466	5	476	4
S2-00_5IR[a]	0.05415	0.0005	0.45201	0.0055	0.06054	0.0008	0.01955	0.0002	377	23	379	4	379	5	391	4
S2-00_5C[a]	0.05693	0.0007	0.58974	0.0085	0.07524	0.0010	0.02221	0.0003	489	29	471	5	468	6	444	7
S2-00_22[a]	0.06081	0.0010	0.85402	0.0153	0.10187	0.0014	0.03203	0.0004	633	37	627	8	625	8	637	8
S2-00_23[a]	0.058	0.0006	0.4132	0.0052	0.05167	0.0007	0.03229	0.0004	530	22	351	4	325	4	642	7
S2-00_60R[a]	0.05917	0.0006	0.42019	0.0050	0.05152	0.0006	0.11887	0.0012	573	22	356	4	324	4	2,270	22
S2-00_66R[a]	0.07181	0.0008	0.16705	0.0016	1.6546	0.0186	0.0524	0.0005	980	24	996	9	991	7	1,032	10
S2-00_90[a]	0.14132	0.0015	8.26378	0.1060	0.42422	0.0055	0.11297	0.0012	2,243	19	2,260	12	2,280	25	2,163	22
S2-00_106[a]	0.05642	0.0009	0.58558	0.0103	0.07525	0.0011	0.01916	0.0003	469	37	468	7	468	6	384	5
S2-00_108[a]	0.05371	0.0008	0.41166	0.0065	0.05556	0.0008	0.01696	0.0012	359	32	350	5	349	5	340	23
Stromatic migmatite																
FD47-1[a]	0.05634	0.0007	0.58308	0.0083	0.0751	0.0009	0.02912	0.0006	466	30	466	5	467	6	580	11
FD47-10[a]	0.06273	0.0007	0.98407	0.0130	0.11379	0.0014	0.0399	0.0004	699	25	696	7	695	8	791	9
FD47-45[a]	0.05636	0.0007	0.59103	0.0079	0.07609	0.0009	0.02609	0.0004	467	26	472	5	473	6	521	8
FD47-64[a]	0.06618	0.0009	1.22943	0.0174	0.13472	0.0017	0.04743	0.0007	812	28	814	8	815	9	937	14
FD47-70[a]	0.05625	0.0007	0.57537	0.0080	0.07418	0.0009	0.02517	0.0005	462	29	461	5	461	5	502	10
Migmatite																
F17-2_1-4-C[b]	0.05612	0.0006	0.59832	0.0059	0.07745	0.0007	n.a.	n.a.	457	25	476	4	481	4	–	–
F17-2_2-3C[b]	0.10313	0.0012	4.09202	0.0537	0.28854	0.0035	n.a.	n.a.	1681	21	1653	11	1,634	17	–	–
F17-2_2-10 C[b]	0.0559	0.0006	0.57508	0.0070	0.07461	0.0008	n.a.	n.a.	448	24	461	5	464	5	–	–
F17-2_5-17C[b]	0.05905	0.0008	0.63574	0.0094	0.07821	0.0009	n.a.	n.a.	569	29	500	6	486	6	–	–

Analysis	Corrected ratios									Corrected ages (Ma)						
	$^{207}Pb/^{206}Pb$	1σ	$^{207}Pb/^{235}U$	1σ	$^{206}Pb/^{238}U$	1σ	$^{208}Pb/^{232}Th$	1σ	$^{207}Pb/^{206}Pb$	1σ	$^{207}Pb/^{235}U$	1σ	$^{206}Pb/^{238}U$	1σ	$^{208}Pb/^{232}Th$	1σ
Diatexite																
S2-00_23[a]	0.05551	0.0010	0.3966	0.0051	0.0518	0.0007	0.016	0.0006	433	41	339	4	326	4	322	13
S2-00_60R[a]	0.05292	0.0009	0.3786	0.0048	0.0519	0.0006	0.016	0.0029	325	40	326	4	326	4	321	58
S2-00_63[a]	0.05681	0.0012	0.4186	0.0066	0.0534	0.0007	0.0162	0.0072	484	47	355	5	336	4	326	142
S2-00_109[a]	0.05406	0.0010	0.399	0.0052	0.0535	0.0007	0.0167	0.0038	373	43	341	4	336	4	334	76

C core, *R* rim, *IR* inner rim

Analyses performed with: [a]213 nm LAM-ICPMS at the GEMOC key Centre, Macquarie University, Sydney; [b]213 nm LAM-ICPMS at CNR- Istituto di Geoscienze e Georisorse Pavia, Italy

Table 2 Selected SHRIMP U–Th–Pb isotope data and calculated ages for zircons from the studied samples (further data available as electronic supplementry material)

Analysis	U (ppm)	Th (ppm)	Th/U	Pb* (ppm)	Total ratios								Age (Ma)	
					$^{204}Pb/^{206}Pb$	f_{206} %	$^{238}U/^{206}Pb$	1σ	$^{207}Pb/^{206}Pb$	1σ	$^{206}Pb/^{238}U$	1σ		1σ
Orthogneiss														
AP16_1.1	174	28	0.16	11.2	0.000260	0.16	13.307	0.156	0.0577	0.0011	0.0750	0.0009	466.4	5.4
AP16_2.1	706	171	0.24	42.8	0.001086	2.09	14.168	0.125	0.0724	0.0014	0.0691	0.0006	430.8	3.8
AP16_4.1	505	44	0.09	32.3	0.000064	< 0.01	13.419	0.123	0.0559	0.0006	0.0746	0.0007	463.6	4.2
AP16_8.1	316	81	0.26	20.1	0.000084	0.10	13.487	0.136	0.0570	0.0008	0.0741	0.0008	460.7	4.6
AP16_14.1	293	138	0.47	27.3	0.000219	< 0.01	9.213	0.093	0.0611	0.0007	0.1086	0.0011	664.8	6.5
AP16_19.1	437	68	0.16	27.9	0.000095	0.01	13.444	0.129	0.0564	0.0007	0.0744	0.0007	462.4	4.4
Diatexite														
S2-00_2.1	263	29	0.11	16.7	0.000156	0.16	13.524	0.141	0.0575	0.0008	0.0738	0.0008	459.2	4.7
S2-00_3.1	257	8	0.03	16.4	0.000192	0.21	13.483	0.174	0.0579	0.0009	0.0740	0.0010	460.3	5.8
S2-00_3.2	80	37	0.46	11.7	0.000395	< 0.01	5.844	0.084	0.0724	0.0012	0.1713	0.0026	1,019	14
S2-00_4.2	128	15	0.11	42.9	0.000047	< 0.01	2.570	0.028	0.1259	0.0009	0.3920	0.0051	2,132	23
S2-00_5.1	113	105	0.93	9.8	–	0.34	9.837	0.125	0.0633	0.0013	0.1013	0.0013	622.0	7.7
S2-00_6.1	197	135	0.69	18.3	0.000171	0.08	9.260	0.099	0.0623	0.0012	0.1079	0.0012	660.5	7.0
S2-00_7.1	1,516	24	0.02	77.9	0.000078	< 0.01	16.727	0.138	0.0540	0.0004	0.0598	0.0005	374.4	3.0
S2-00_8.1	319	65	0.20	20.6	0.000040	0.05	13.348	0.135	0.0568	0.0008	0.0749	0.0008	465.5	4.6
S2-00_9.1	215	16	0.08	13.7	0.000205	0.15	13.498	0.193	0.0574	0.0011	0.0740	0.0011	460.0	6.5

The heterogeneity of the zircon textures and shapes reflects the spread of U/Pb ages in the Concordia diagram from about 3 Ga to 349 Ma (Fig. 4b). A total of 87 analyses were performed on 65 different zircon crystals by means of LAM-ICPMS. The largest zircon population (21 of a total of 78 concordant LAM-ICPMS analyses) clusters between 501 and 452 Ma, with 16 points defining a well-constrained mean concordant age of 466 ± 2 Ma (MSWD = 1.03). These ages were obtained on homogenous or oscillatory-zoned cores, inner rims of elongated crystals and, more rarely, on oscillatory-zoned equant grains. A smaller group (nine analyses) of younger ages ranging from 449 to 427 Ma was obtained on slightly zoned overgrowths, and four younger ages of 404, 379, 358 and 349 Ma were measured on the two strongly-zoned bright rims and two unzoned rims of small subhedral grains. Other bright domains and rims define a small group (four analyses) of discordant data pointing to even younger ages. The occurrence of fractures and metamict patches in such areas probably favoured their alteration and contamination by common lead. On a Tera–Wasserburg plot, when corrected for common lead with the method proposed by Andersen (2002), they define a lower intercept of 327 ± 23 Ma.

The spread of SHRIMP data (25 analyses) is similar to that of U–Pb data, with the younger ages ranging from 494 to 374 Ma (17 analyses). The age of 464 ± 3.8 Ma (MSWD = 1.4), based on the weighted average of 12 analyses, is comparable to that obtained with the LAM-ICPMS method.

A total of 47 LAM-ICPMS and SHRIMP analyses (39 from LAM-ICPMS, 8 from SHRIMP) yielded ages older than 501 Ma: 32 of them define a group of Neoproterozoic ages ranging from 680 to 555 Ma. The oldest Neoproterozoic ages were obtained for weakly-zoned to unzoned short-prismatic and subrounded zircons; the relatively younger ones were often measured in the zoned cores of elongated grains. The remaining 15 ages scatter between 787 and 3 Ga, with small groups around 1 and 2 Ga. Ages older than 2 Ga pertain to subrounded and unzoned zircon grains.

Stromatic migmatite FD47

Like in the S2-00 diatexite, zircons of the FD47 stromatic migmatite show a variety of shapes ranging from euhedral–elongated crystals to short-prismatic, equant euhedral to rounded grains. Internal structures also vary considerably, ranging from euhedral oscillatory zoning to convoluted zones, ghost zones and unzoned domains (Fig. 3). Relic cores with or without oscillatory zoning are often present. Concordant U–Pb ages span between 814 and 450 Ma (39 analyses). The total weighted average of the 32 analyses, younger than 500 Ma, gives an age of 466 ± 3.3 Ma (MSWD = 3.3). Older concordant ages spread between 814 and 533 (seven analyses), with a small peak of Neoproterozoic data clustering around 596 Ma (Fig. 4c).

Paragneiss F17-2

In the F17-2 paragneiss euhedral short-prismatic grains predominate over elongated ones, and the majority of grains have subrounded edges. Internal structures vary from oscillatory growth zoning to sector zoning (Fig. 3). Evidence of overgrowth at the rim is frequent, and several grains contain subrounded and partially resorbed cores with complex internal structures. Concordant ages are scattered and range between 1.65 Ga and 393 Ma (Fig. 4d). The largest zircon population (14 of

Table 3 Representative trace element contents (ppm) of analysed zircons after LAM-ICPMS analyes (further data available as electronic supplementary material)

Sample	S2-00_60R	S2-00_5R	S2-00_5R	S2-00_108R	S2-00_2C	S2-00_15C	S2-00_44	S2-00_33	S2-00_7	S2-00_39	AP16_130	AP16_143R
Age (Ma)	325[a]	379 ± 4	379 ± 4	349 ± 5	468 ± 5	467 ± 6	460 ± 5	607 ± 7	613 ± 7	2,050 ± 8.3	462 ± 4	458 ± 4
Element (ppm)												
Ti	918.55	8.63	4.4	< 3.77	< 11.41	16.34	< 4.36	25.64	8.94	18.27	9.99	< 4.11
Sr	71.97	14.61	14.15	1.11	0.25	0.522	0.215	0.084	0.58	< 0.068	< 0.086	0.99
Y	10,016.37	3122	3268.1	1076.43	1,392.77	4,584.21	2,743.99	680.29	782.07	134.04	805.94	822.76
Nb	11.95	11.04	6.51	2.68	4.57	2.47	2.83	3.47	2.51	2.15	5.29	4.40
Ba	56.65	8.29	6.81	< 0.137	< 0.00	0.98	< 0.228	< 0.27	1.18	< 0.158	0.65	1.03
La	119.14	17.41	16.77	2.15	0.285	0.027	< 0.044	0.036	1.44	< 0.025	< 0.045	0.89
Ce	342.9	68.07	69.54	3.62	1.79	0.704	0.362	24.22	13.23	2.33	15.23	6.94
Pr	59.21	16.52	14.78	0.68	0.062	0.105	< 0.0242	0.061	0.64	0.088	< 0.00	0.54
Nd	838.51	94.73	91.75	5.03	1.18	1.32	0.44	1.25	3.07	0.61	0.95	3.32
Sm	300.71	71.02	71.38	6.54	4.21	9.94	3.12	4.3	2.82	2.33	1.45	4.46
Eu	63.32	24.71	19.33	1.68	0.143	0.04	0.277	0.49	1.04	0.146	0.31	0.71
Gd	374.8	175.16	150.85	16.62	19.58	58.59	25.16	17.47	18.43	12.44	17.20	16.78
Tb	117.29	56.26	47.52	8.39	9.96	28.73	14.48	5.21	5.42	2.82	6.10	7.07
Dy	968.58	422.51	428.35	109.95	124.85	377.24	218.04	65.07	63.31	23.2	71.27	80.44
Ho	272.7	100.89	120.08	35.61	45.45	159.73	90.81	22.72	25.56	5.04	28.46	27.63
Er	935.65	306.47	457.1	155.35	202.7	704.07	426.67	99.86	126.61	14.84	132.50	117.27
Tm	199.75	54.72	93.48	34.78	41.11	158.91	102.25	20.8	28.36	2.26	28.23	25.35
Yb	1,624.27	439.57	892.76	321.34	401.54	1,513.51	1,029.77	206.85	301.15	16.02	296.65	248.13
Lu	281.59	63.66	139.18	47.13	73.57	225.26	166.08	34.7	50.8	1.96	47.02	41.57
Hf	9,564.67	12,759.81	10,600.63	10,170.94	14,791.38	11,761.89	11,130.73	10,788.06	14,082.55	12,906.15	10,456.99	10,069.10
Ta	4.17	9.09	3.78	0.57	1.25	0.768	0.456	0.432	0.89	0.209	1.96	1.53
Pb	46.83	6.17	21.09	1.84	1.93	3.15	1.24	21.76	7.74	17.25	38.76	4.98
Th	475.65	12.47	298.4	23.49	72.94	81.02	28.3	167.56	89.79	89.3	160.22	87.74
U	2,197.07	2,281.99	1,484.29	387.04	550.71	338.09	351.05	196.02	234.45	210.98	367.51	348.84
Th/U	0.2164929	0.0054645	0.2010389	0.0606914	0.1324472	0.2396403	0.0806153	0.8548107	0.3829814	0.4232629	0.4359609	0.2515193
REE_{TOT}	6,498.42	1,911.7	2,612.87	748.87	926.43	3,238.176	2,077.459	503.037	641.88	84.084	645.371	581.098

[a]After common lead correction; analyses performed with a 213 nm LAM-ICPMS at CNR-Istituto di Geoscienze e Georisorse of Pavia, Italy

Table 4 Selected LAM-ICPMS Lu and Hf isotope data and calculated model ages for dated zircons (further data available as electronic supplementry material)

Analysis	Age (Ma)	$^{176}Lu/^{177}Hf$	$^{176}Yb/^{177}Hf$	$^{176}Hf/^{177}Hf$	1σ	TDM (Ga)	TDM crustal (Ga)	$^{176}Hf/^{177}Hf$ initial	εHf
S2-00_2	477	0.000693	0.029194	0.282512	0.000008	1.00	1.34	0.282506	1.2
S2-00_3	466	0.001155	0.049307	0.282566	0.000012	0.94	1.23	0.282556	3.0
S2-00_7	613	0.000559	0.022654	0.282499	0.000012	1.02	1.28	0.282492	4.1
S2-00_22	626	0.000651	0.026604	0.282768	0.000015	0.66	0.68	0.282760	13.9
S2-00_23	320	0.005496	0.212504	0.282615	0.000015	0.99	1.27	0.282581	0.5
S2-00_24	2,988	0.000321	0.012942	0.280934	0.000013	3.06	3.11	0.280915	4.1
FD47_1	467	0.002247	0.092549	0.282458	0.000017	1.12	1.49	0.282438	−1.2
FD47_3	595	0.000604	0.023022	0.282076	0.000020	1.58	2.20	0.282069	−11.3
FD47_10	696	0.001060	0.032361	0.282801	0.000011	0.62	0.57	0.282787	16.4
FD47_11	533	0.001304	0.053408	0.282257	0.000014	1.37	1.87	0.282244	−6.6
FD47_12	450	0.001520	0.061274	0.282629	0.000012	0.87	1.11	0.282616	4.7
FD47_23	461	0.001569	0.064969	0.282498	0.000013	1.05	1.39	0.282484	0.3
FD47_27	484	0.001480	0.058218	0.282477	0.000011	1.07	1.42	0.282463	0.1
FD47_64	814	0.001028	0.034491	0.282570	0.000018	0.93	1.01	0.282554	10.9

Analyes performed with 213 nm LAM-ICPMS at the GEMOC Key Centre, Macquarie University, Sydney

32 analyses) yields ages of 505–462 Ma. These ages generally refer to zircon cores with well-developed oscillatory zoning. Ten of 32 concordant points are older than 500 Ma, with one defining an age of 1.65 Ga and seven defining Neoproterozoic ages of 664–554 Ma. Nine zircons scatter between 443 and 393 Ma. All these younger ages, except two, were usually obtained from the rim of zircons with complex zoning patterns and evidence of overgrowths.

Lastly, the analysed orthogneiss and the meta-rhyodacite show a large prevalence of ages spanning from 480 to 450 Ma (about 70% of the concordant ages) with a clear peak around 460–470 Ma. Such ages are mostly obtained from euhedral zircons with oscillatory zoning. Few younger (>380 Ma) and older ages (<770 Ma) are usually restricted to the rims and inherited cores, respectively. Zircons from metasediments show more heterogeneous age spectra: the main cluster (42%) of about 160 concordant ages spans from 480 to 450 Ma. These ages are predominantly obtained from euhedral to subhedral zircon grains. Ages from about 550 to 650 Ma form a second main peak (16%) and relate to single zircon grains or core portions with variable shapes and internal textures. Ages older than 650 Ma up to 2.9 Ga are very scattered and were always obtained from rounded zircon grains or inherited cores. Finally, ages younger than 400 Ma are rare (<4%), usually found at zircon rims.

Zircon rare earth and trace element composition

In order to better interpret the meaning of U/Pb ages, we determined the trace element composition of dated zircons. Ablation pits were usually sited near the spot U/Pb analyses, and the results are shown in Table 3 and Fig. 5a.

The Th/U ratios of euhedral grains with magmatic oscillatory zoning and Middle Ordovician to Neoproterozoic ages (the two main age clusters at ~470 and 650–580 Ma) are usually greater than 0.2. Chondrite-normalised rare earth element patterns exhibit high fractionation of LREEs over HREEs ($La_N/Yb_N < 0.0002$) and marked negative Eu anomalies ($Eu/Eu^* = 0.03 - 0.3$). The bright rims of a few grains (younger than 450 Ma) were difficult to analyse because of their small dimensions and the presence of fractures and inclusions. Several analyses were discarded due to anomalous concentrations (up to hundreds of ppm) of trace elements such as B, Na, Ba, Ca and Mg, suggesting the presence of inclusions or impurities within the cracks. The analyses considered representative of zircon compositions have flatter REE patterns, a weak or absent negative Eu anomaly, and $La_N/Yb_N > 0.001$. The concentrations of the other trace elements are rather variable, but the Th/U ratio is usually less than 0.2.

The analyses of inherited cores and zircons older than 700 Ma yielded heterogeneous results linked to variations in the observed internal microstructures and are not considered in detail in this work.

Magmatic versus metamorphic zircons

The euhedral shapes, the oscillatory zoning observed in BSE and CL images and the trace element compositions with negative Eu anomalies and high Th/U ratios suggest that the zircons with Middle Ordovician to Neoproterozoic ages formed under magmatic conditions (Hinton and Upton 1991; Hanchar and Miller 1993). Zircons with such characteristics form the largest populations in both the granitic orthogneiss (AP16) and the three paragneisses (S2-00, FD47 and F17-2). Some features of the bright rims with younger ages found in a few zircons of the S2-00 migmatite and the AP16 orthogneiss point to a metamorphic origin: the lack of zoning and the low Th/U ratios are typical of metamorphic zircons in the literature (Hoskin and Black 2000).

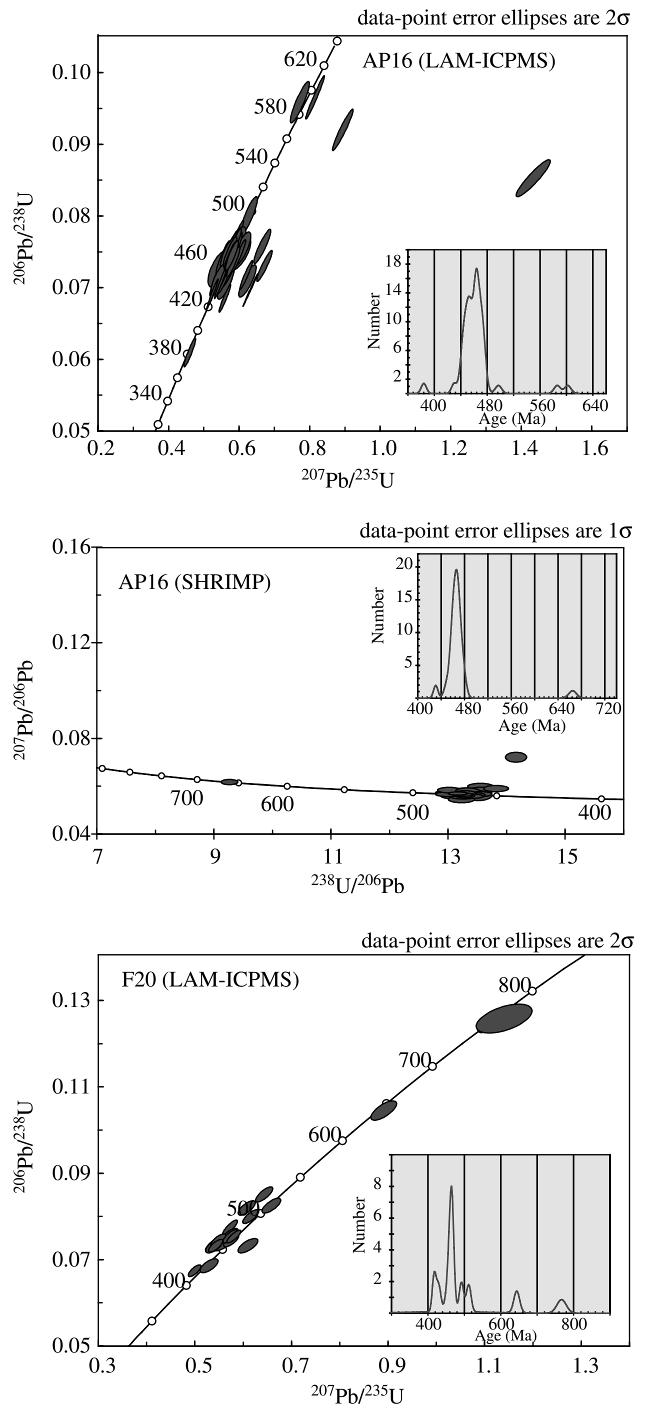

Fig. 4 LAM-ICPMS and SHRIMP U/Pb zircon ages plotted on Concordia, Tera–Wasserburg and density diagrams: **a** orthogneiss AP16 and meta-rhyodacite FA206, **b** diatexite S2-00, **c** stromatic migmatite FD47, **d** paragneiss F17-2

U/Pb geochronology therefore reveals that both sedimentary and magmatic protoliths record a main zircon-forming event in the Middle to Late Ordovician times. In particular, the zircon population in the granitic orthogneiss clearly constrains the emplacement age of the magmatic protolith to 466–469 Ma (SHRIMP and LAM-ICPMS data). A slightly younger age of 460 ± 5 Ma was recently proposed (Giacomini et al. 2005) for the emplacement of the magmatic eclogite protoliths in the Golfo Aranci area. In accordance with this emplacement age, the youngest detrital zircons with magmatic textures in the paragneisses suggest a derivation from dominantly Middle Ordovician magmatic rocks.

The Variscan metamorphic history of the studied felsic gneisses is poorly constrained by zircon geochronology. Even though the analysed samples display evidence of high-temperature metamorphic overprint up to migmatite development (Carmignani et al. 1992; Ricci et al. 2004), zircon resetting and recrystallisation are generally limited to thin rims in older zircons. The large scatter of metamorphic ages between about 450 and 320 Ma is unlikely the result of long-lasting re-equilibration. Even if old metamorphic ages cannot be excluded a priori, we suggest that ages older than 360 Ma probably result from the mixed sampling of older inner portions of zircon and younger thin rims. Alternatively, such ages could be the result of the partial inhomogeneous resetting of zircons (possibly related to metamict processes) during the subsequent metamorphic evolution.

In contrast, after comparison with published data on the Sardinian metamorphic basement, we suggest that all ages younger than 360 Ma and the slightly discordant analyses with a lower intercept pointing to 330–320 Ma can be realistically considered the result of the high-temperature partial resetting of zircons. Indeed, metamorphic zircons from amphibolitised eclogites embedded within the felsic gneisses of the Sardinian basement yielded recrystallisation ages of 350–320 Ma (Palmeri et al. 2004; Giacomini et al. 2005). Moreover, migmatite formation in northern Sardinia is constrained to 344 Ma (Rb/Sr whole rock, Ferrara et al. 1978), in good agreement with the maximum thickening stage of the basement inferred from the Ar/Ar dating of high-celadonite micas from the garnet zone (about 340 Ma ago, Di Vincenzo et al. 2004).

Lu–Hf isotope data

Selected zircons from S2-00 and FD47 were analysed not only for U–Pb but also for the Hf isotope composition. The isotopic composition of Hf in zircon is an indicator of crustal evolution (Vervoort and Patchett 1996; Bodet and Schärer 2000; Andersen et al. 2002); it helps to constrain the age and nature of different crustal components recycled by sedimentary rocks.

Ablation spots for Hf analyses were sited near the spots used for the U–Pb isotope analyses (Fig. 3). Table 4 reports analytical data, as well as time-corrected ^{176}Hf/^{177}Hf and initial epsilon-Hf values for each grain. Given the small size of zircons and the need to link the Hf isotopic composition to the U–Pb age, a limited number of analyses were obtained for the older inherited

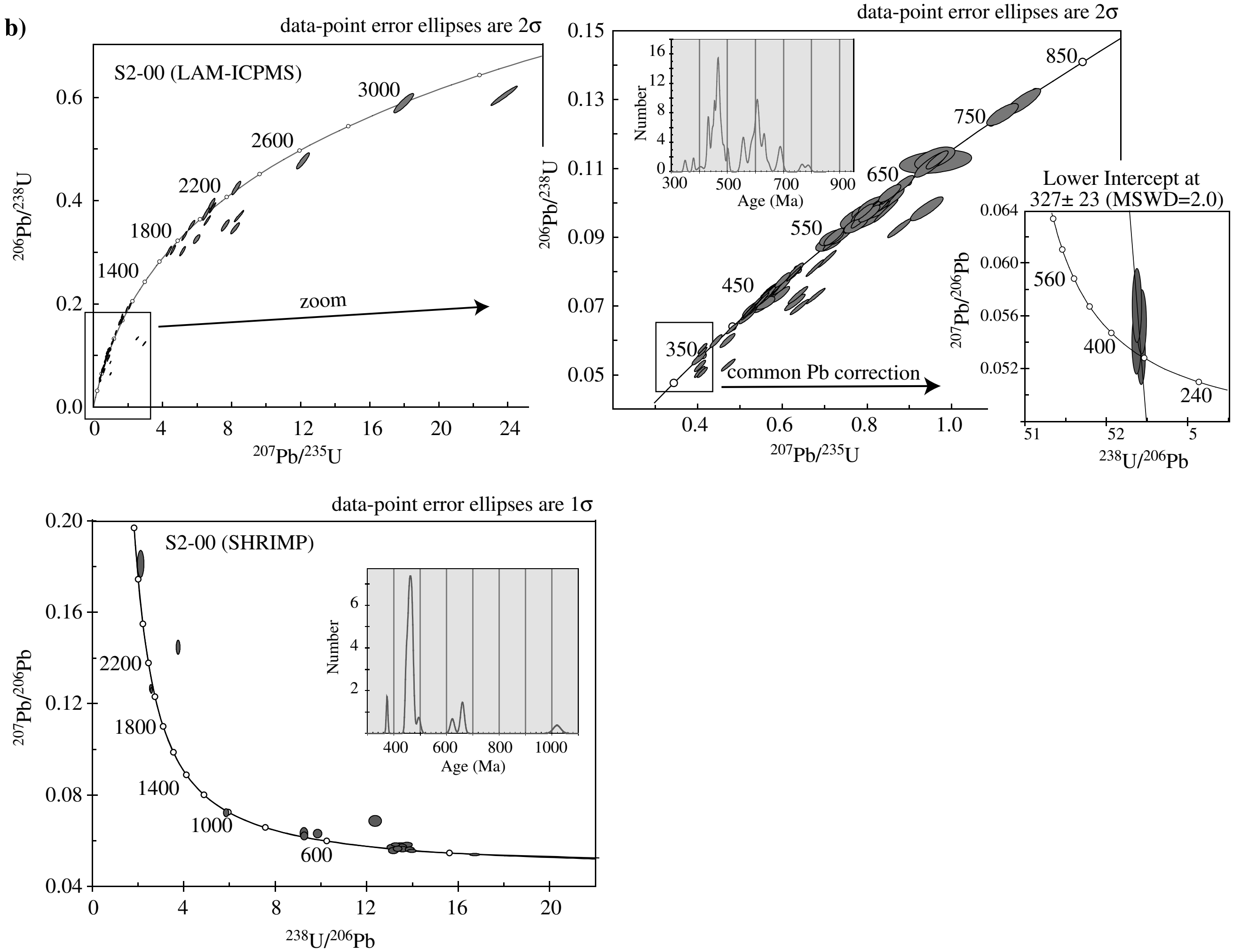

Fig. 4 (Contd.)

components, which often occur as small rounded cores. The obtained ^{176}Hf/^{177}Hf data were plotted against age in Fig. 5b, which also reports the evolution curves of the depleted mantle and CHUR.

The main zircon population is about 460 Ma old. The Hf isotope composition ranges from 0.282427 ± 0.000024 (2σ) to 0.282629 ± 0.000024 in sample FD47 and from 0.282433 ± 0.000016 to 0.282566 ± 0.000044 in sample S2-00, defining a cluster intermediate to the values expected for a chondritic reservoir and those expected for zircons crystallised from magmas with a depleted mantle source. These ratios correspond to εHf values ranging from −2.6 to 4.7 and from −1.7 to 3.0 in FD47 and S2-00, respectively. The scatter in the ^{176}Hf/^{177}Hf ratios is greater than the analytical uncertainty. This can be explained by a relative heterogeneity in the zircon population including components formed by the re-melting of distinct sources with different ages and Lu/Hf ratios. Alternatively, the ^{176}Hf/^{177}Hf scatter may be due to crystallisation from magma generated from a depleted mantle source that interacted with crustal material depleted in radiogenic Hf. The first model is supported by the wide variety of ages and Hf isotope compositions in sample S2-00. On the other hand, the absence of ^{176}Hf/^{177}Hf values approaching the depleted mantle evolution line and that of the strongly negative εHf values, together with the strong similarity between the ^{176}Hf/^{177}Hf ratios of S2-00 zircons and those of FD47 (poorer in old components), seem to support the second hypothesis. Zircon domains in sample S2-00 with ages of 430 and 320 Ma have ^{176}Hf/^{177}Hf ratios in the same range.

Crustal residence ages were constrained assuming two different ^{176}Lu/^{177}Hf values. The first value is equivalent to a depleted mantle source representing minimum ages for the parent magma from which zircons crystallised; the second is equivalent to an average crustal protolith obtained assuming a typical crustal Lu/Hf ratio (Griffin et al. 2000; Andersen and Griffin 2004). The crustal residence age for a depleted mantle protolith (^{176}Lu/^{177}Hf = 0.0384) ranges from 0.87 to 1.18 (mean value = 1.04) in sample FD47 and from 0.94 to 1.03

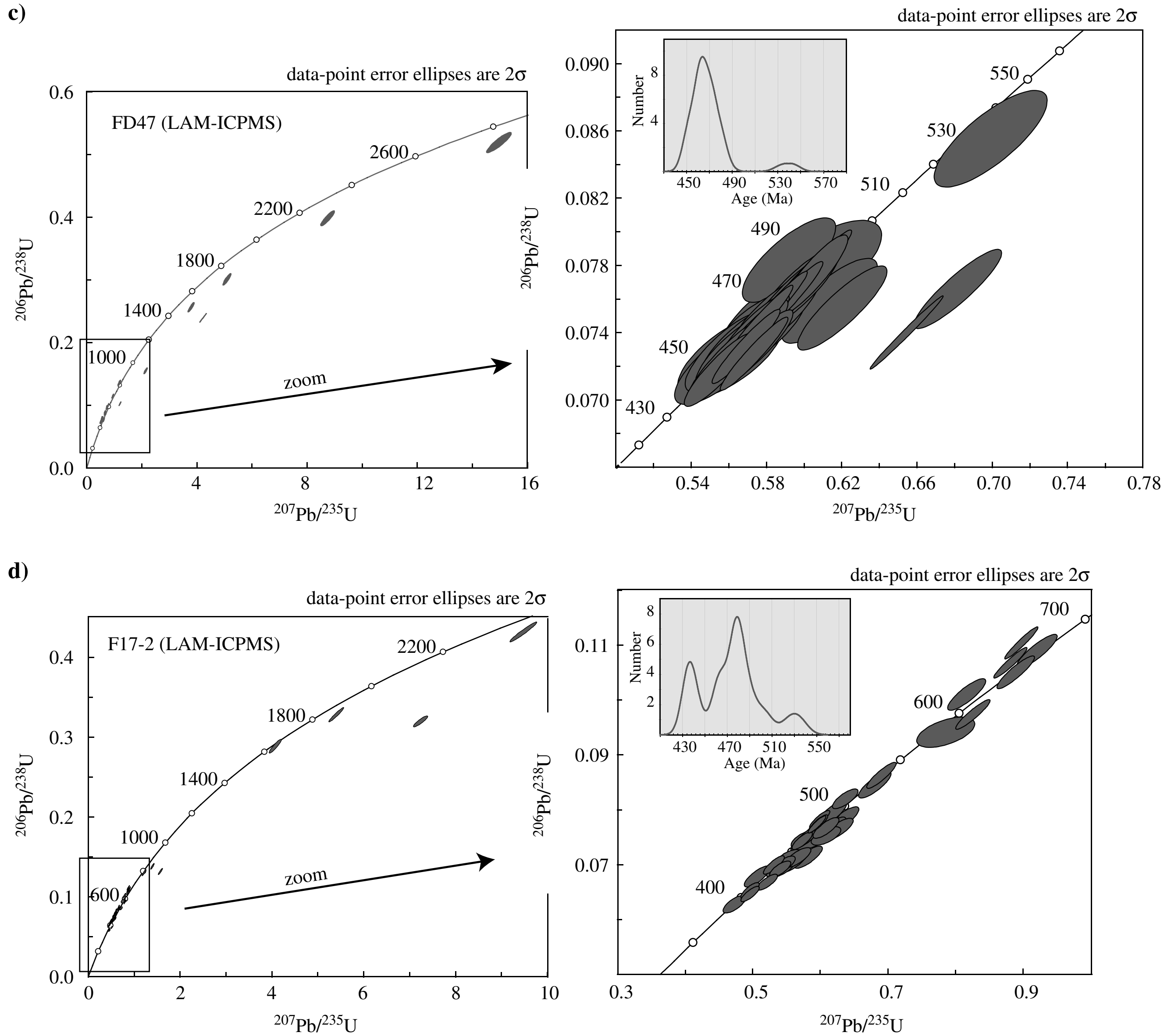

Fig. 4 (Contd.)

(mean value = 1.03) in sample S2-00. Assuming an average crustal source ($^{176}Lu/^{177}Hf$ = 0.015), the T_{DM} of sample FD47 is 1.11–1.57 (mean value = 1.38) and the T_{DM} of sample S2-00 is 1.23–1.52 (mean value = 1.38).

The zircon population with U–Pb ages of around 600 Ma defines a scattered cluster in the $^{176}Hf/^{177}Hf$ versus age plot, with the $^{176}Hf/^{177}Hf$ ratios ranging from values lying on the depleted mantle evolution line at the time and non-radiogenic Hf values (Fig. 5b).

Zircons from the two samples are similar, with values ranging from high radiogenic Hf values near or slightly above the depleted mantle evolution line ($^{176}Hf/^{177}Hf$ = 0.282801, εHf = 16.4) to a low $^{176}Hf/^{177}Hf$ ratio of 0.28195 (εHf = −15.9). The wide scatter of the $^{176}Hf/^{177}Hf$ ratios suggests a heterogeneous origin for this older zircon population: the presence of zircons with high $^{176}Hf/^{177}Hf$ ratios near the DM evolution line indicates the production of juvenile melts around 600 Ma ago, but the presence of strongly negative εHf values also points to the production of magmatic rocks with crustal affinity.

The most radiogenic Hf composition (0.282801) in sample FD47 lies above the depleted mantle evolution line (bold cross in Fig. 5b) and is similar to the most radiogenic composition in sample S2-00. The complexity of the zircon grain (a zoned relic core overgrown by a likely younger mantle) that yielded this composition suggests the mixing of two components: an older component with a less radiogenic Hf isotope composition, and a younger (600 Ma old) zircon domain crystallised from a magma that originated from a depleted mantle source.

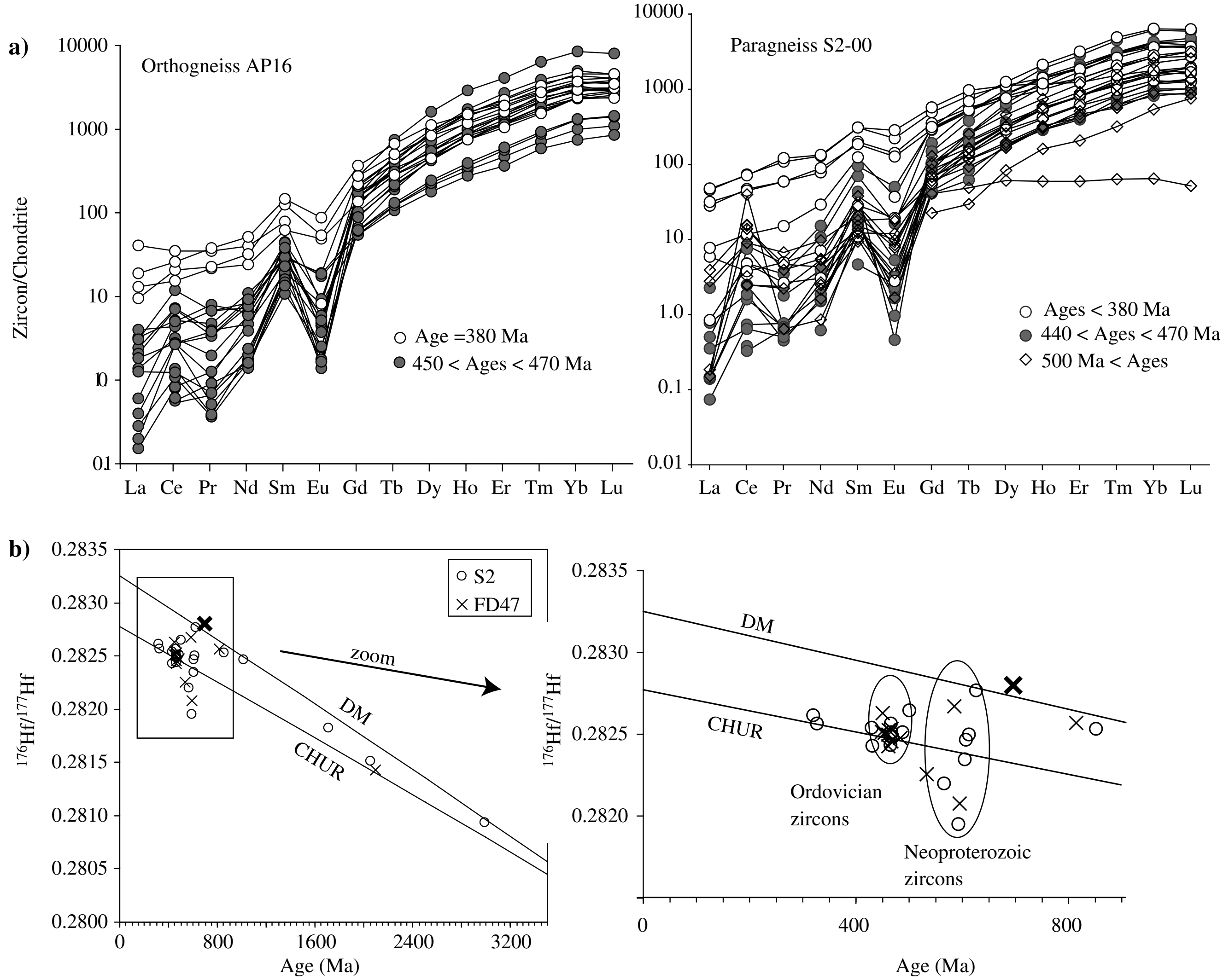

Fig. 5 **a** Zircon/chondrite-normalised REE patterns of selected zircons from samples AP16 (*left*) and S2-00 (*right*); **b** $^{176}Hf/^{177}Hf$ data from selected zircons of S2-00 and FD47 plotted against U/Pb age; zoom on the Early Palaeozoic and Neoproterozoic zircon populations on the right

Numerous episodes of more recent continental crust extraction are documented, and the production of juvenile melts is also recorded in two zircons, respectively, 1 and 3 Ga old.

In conclusion, the results of U/Pb, Lu/Hf and trace element analyses on zircons from the Sardinian metamorphic rocks can be summarised as follows.

- The chemical composition and textures of zircons with Ordovician ages indicate formation under magmatic conditions; Lu/Hf data indicate crustal residence ages of about 1 Ga.
- Ordovician zircons represent the dominant population found in the felsic orthogneiss as well as in the migmatitic paragneisses of northern Sardinia and in the metarhyodacite from southern Sardinia.
- Older zircons and inherited cores are common in the metasediments and indicate the multiple recycling of older crust, particularly of Cadomian age.
- Zircon ages younger than 400 Ma are rare and predominantly found at zircon rims; the combined trace element and textural analyses suggest that these ages are related to the U/Pb system resetting or new zircon crystallisation during metamorphic events of Variscan age.

Geochemistry

Major and trace elements

The geochemical characterisation of metamorphic rocks from the Sardinian basement must be applied with caution: indeed the majority of analysed samples come from northern Sardinia and were metamorphosed under amphibolite to granulite facies conditions. Therefore, they likely experienced some element mobility, particularly if partial melting reactions induced the escape of melt from the source rock. Table 5 reports the composition of representative gneisses from NE Sardinia (39 analyses); orthogneisses and metavolcanics from central-southern Sardinia (12 analyses), as well as eight metasediments and one orthogneiss from southern Corsica were also analysed for comparison. For the complete set of analyses refer to Tables 14–18 (electronic supplementary material).

Orthogneisses

The metagranitoids from the Golfo Aranci area have high-K calcalkaline compositions; both muscovite garnet-bearing peraluminous granites and hornblende-bearing metaluminous granodiorite–tonalites occur in the area. SiO_2 ranges from 73 to 61 wt%, and the analysed samples fall between the rhyodacite and rhyolite fields in the SiO_2 versus Nb/Y diagram (Fig. 6a). Using the discrimination diagrams of Pearce et al. (1984), all analysed granitoids plot within the volcanic arc granite field (Fig. 6b). The MORB-normalised trace element patterns, with small or absent negative Ba anomalies with respect to Rb and Th, and the slight depletion in HFS elements are similar to those of typical volcanic arc and collisional granites (Fig. 6c). No compositional difference can be seen between the pre-Variscan magmatic rocks from the Golfo Aranci area and those from the Sardinian nappe zones and other basement slices in the Italian peninsula (e.g. Atzori et al. 2003; Mazzoli et al. 2003).

Metasediments

The geochemical composition of clastic sedimentary rocks depends on several factors such as provenance, weathering and duration of transport (e.g. Bathia 1983).

All metasedimentary rocks from the northern Sardinia basement are immature, quartz-rich clastic sediments, mainly wackes to arkoses with subordinate pelites (Fig. 7a, b: classification after Wimmenauer 1984). Following the classification of Floyd and Leveridge (1987), the analysed migmatite samples plot within the ‘‘acidic arc source’’ field, thus suggesting an origin from the weathering and erosion of felsic magmatic rocks (Fig. 7c). The discrimination diagrams of Bathia (1983), Bathia and Crook (1986) and Plank (2005) indicate that the analysed rocks have a ‘‘continental island arc’’ and ‘‘active continental margin’’ affinity (Fig. 7d, e), with the Th/La ratios always greater than 0.2 (Fig. 7d, e, f).

Sr and Nd Isotopic composition

Whole rock Sr and Nd isotopic ratios of one representative orthogneiss (AP16) and three paragneisses (S1-99, S2-00, FD47) were also measured. An average formation age of 470 Ma was assumed for all lithologies. The measured isotopic ratios are similar for all the analysed samples: $(^{143}Nd/^{144}Nd)_{470\ Ma}$ ranges from 0.51175 to 0.51181, with an $\varepsilon_{Nd\text{-}470\ Ma}$ of −7.7 to −9.9. $(^{87}Sr/^{86}Sr)_{470\ Ma}$ is rather homogeneous for three samples, ranging between 0.70954 and 0.71056. Sample FD47 has a very low $(^{87}Sr/^{86}Sr)_{470\ Ma} = 0.705396$, which is most likely due to Rb and Sr mobilisation during the Variscan metamorphic evolution.

The measured Sr and Nd isotopic ratios are in agreement with those published by Di Vincenzo et al. (1996) for one orthogneiss from the same outcrop as sample AP16 and two orthogneisses from the Lodè complex (Sardinia); they demonstrate that orthogneisses and paragneisses mainly derive from a relatively young felsic-to-intermediate crust: T_{CHUR} model ages fall in the 950–1,050 Ma range. This is also in agreement with the main age clustering of the Precambrian zircon population in the paragneisses, where grains with ages of 550 Ma to 1.0 Ga largely prevail over those older than 1.0 Ga.

Discussion

The Variscan polyphase metamorphic overprint that affected the northern Sardinian basement hampers an accurate reconstruction of the pre-Variscan structure of the crust in the area. Nevertheless, collected data and recently published papers (Helbing 2003; Cortesogno et al. 2004; Palmeri et al. 2004; Helbing and Tiepolo 2005; Giacomini et al. 2005) provide new constraints for understanding the Palaeozoic evolution of this basement.

The Early Palaeozoic magmatism

A widespread production of both granitic and basaltic magma is attested throughout the Sardinian crust in the Middle Ordovician.

The *felsic* orthogneiss of Golfo Aranci, dated by in-situ U/Pb zircon geochronology (470–465 Ma), represents shallow level intrusions of subalkaline magmas with granite–granodiorite–tonalite compositions.

In central-southern Sardinia the thick calcalkaline metavolcanic sequences and the intrusive orthogneisses of Lodè, Tanaunella, S. Lorenzo and Capo Spartivento, as well as the Corsican orthogneisses of Zicavo and Portovecchio (Carmignani and Rossi 2001), can be considered co-magmatic, nearly coeval to those of the Golfo Aranci area, although there is some uncertainty on the ages constrained by geochronological studies (480–450 Ma: Delaperrière and Lancelot 1989; Ludwig and Turi 1989; Carmignani 2001; Helbing 2003; Helbing and Tiepolo 2005). The U/Pb zircon ages of 464 ± 1 Ma obtained from a typical metarhyodacite from Sarrabus (sample F20) and the data published by Garbarino et al. (2005) confirm these results.

Table 5 Chemical analyses of representative ortho- and paragneisses from the NE-Sardinian basement (further data available as electronic supplementry material)

Sample	11X3a	AP-16	AP 26	AP-15	AP 28	*Average*	H-373	GFS415	H-163	S4-99	F17-2	FD36	FD47	GFS417	S2-00	S1-00	S1-99	S3-99	H-168	S2-99	*Average*
Lithotype	Orthogneisses						Paragneisses														
Area	Bados	Golfo Aranci				11 samples	Golfo Aranci														23 samples
Wt%																					
SiO_2	64.09	70.86	71.05	71.84	72.24	70.84	52.45	62.58	64.49	64.97	65.73	68.44	68.54	69.45	69.47	69.52	69.70	70.19	70.48	71.32	66.33
TiO_2	0.59	0.41	0.32	0.29	0.35	0.38	1.09	0.75	0.67	0.73	0.78	0.53	0.53	3.05	0.42	0.41	0.36	0.43	0.46	0.26	0.72
Al_2O_3	16.54	14.59	15.23	14.50	14.07	14.87	22.45	17.27	16.30	16.28	15.47	15.29	15.53	15.23	15.35	15.13	15.58	15.15	15.05	15.45	15.95
Fe_2O_3	1.42	0.32	0.65	0.64	0.55	0.61	4.61	0.81	1.51	0.50	1.32	0.81	2.86	0.53	0.39	0.32	0.84	0.08	0.78	0.21	1.11
FeO	3.89	2.63	1.85	1.72	1.98	1.93	4.90	4.80	4.31	4.16	4.40	2.99	0.86	2.90	2.98	3.04	2.13	3.17	2.94	1.84	3.64
MnO	0.10	0.04	0.04	0.03	0.04	0.04	0.12	0.06	0.09	0.08	0.09	0.04	0.03	0.05	0.04	0.05	0.04	0.06	0.09	< DL	0.07
MgO	2.55	0.85	0.52	0.68	0.61	1.22	3.87	2.07	2.46	1.63	2.72	1.15	1.01	1.31	1.30	1.28	1.07	1.09	1.14	0.76	1.87
CaO	4.85	1.61	1.34	1.32	1.17	1.53	0.28	3.03	4.02	3.88	2.13	1.94	2.42	0.05	1.87	1.68	1.77	2.42	2.65	1.50	2.45
Na_2O	2.92	2.82	3.17	2.69	2.65	2.92	0.84	4.03	3.02	2.84	3.28	3.00	3.34	1.30	3.17	2.97	3.26	3.21	3.39	3.26	2.99
K_2O	2.36	4.23	4.11	5.82	4.94	4.44	4.99	2.67	2.32	3.29	3.01	3.95	3.87	1.70	3.42	3.82	3.45	3.35	3.10	3.86	3.15
P_2O_5	0.15	0.21	0.17	0.22	0.16	0.17	0.17	0.34	0.18	0.18	0.17	0.23	0.20	3.66	0.16	0.17	0.18	0.14	0.14	0.13	0.33
LOI	1.02	1.29	1.27	0.85	1.21	1.06	3.90	1.49	0.87	1.32	1.41	1.17	0.72	0.44	1.30	1.47	1.27	0.67	0.56	1.26	1.33
Total	100.48	99.86	99.72	100.61	99.97	100.00	99.66	99.90	100.25	99.86	100.51	99.54	99.91	99.67	99.87	99.86	99.65	99.96	100.78	99.85	99.93
Ppm																					
Be	2	3	2	2	3	2	4	2	3	2	2	3	3	2	4	6	3	4	3	5	3.22
V	78	32	23	21	22	34	105	115	84	69	111	45	42	60	54	53	39	39	35	33	66
Cr	43	23	18	18	20	25	99	35	71	12	99	30	26	42	42	43	29	26	25	26	44
Co	13	6	4	4	4	6	17	13	12	8	16	7	7	8	9	8	6	6	6	4	11
Ni	12	9	8	8	7	8	39	17	16	< DL	39	13	12	19	19	19	14	8	7	12	18
Cu	6	10	9	8	8	9	33	16	11	< DL	31	12	14	< DL	< DL	6	< DL	8	< DL	9	19
Zn	99	63	61	51	53	58	153	90	92	81	97	78	67	86	83	81	63	64	67	43	86
Ga	20	22	20	19	20	20	30	24	23	23	22	20	20	23	23	21	20	21	20	19	22
Ge	2	1	1	1	1	1	2	2	2	2	2	2	1	2	2	2	2	2	2	2	2
As	< DL	< DL	< DL	1	4	2	2	< DL	< DL	< DL	< DL	1	< DL	1	3	1	2	< DL	< DL	1	2
Rb	108	125	129	172	174	127	276	106	111	132	129	118	100	149	135	135	98	152	123	110	129
Sr	253	150	140	160	93	178	96	293	265	221	256	204	192	192	212	171	213	174	206	225	204
Y	29	49	39	30	47	35	54	24	30	35	32	43	35	27	33	26	32	39	44	29	32
Zr	108	197	152	154	190	132	233	211	199	219	222	273	247	130	156	136	146	195	202	85	178
Nb	7.8	12.4	10.2	9.6	11.6	6.6	16.0	11.0	11.6	12.8	11.8	11.3	12.2	11.4	10.8	10.5	9.1	11.1	11.2	7.6	10
Mo	< DL	0.3	< DL	< DL	0.5	0.4	< DL	0.9	0.9	0.7	1.0	1.0	1.0	0.5	0.8	0.8	0.2	0.3	0.7	0.3	0.8
In	0.1	< DL	0.1	0.1	0.1	0.1	0.1	< DL	0.1	< DL	0.1	< DL	< DL	< DL	< DL	< DL	< DL	0.1	0.1	< DL	0.1
Sn	6.1	2.5	3.5	2.0	3.5	2.9	8.7	2.8	2.2	2.4	2.8	3.2	1.5	4.8	4.4	4.4	3.6	4.2	1.9	3.5	3.4
Sb	< DL	< DL	< DL	< DL	< DL	–	< DL	< DL	< DL	< DL	< DL	< DL	< DL	< DL	0.1	< DL	< DL	< DL	< DL	< DL	0.2
Cs	5.5	3.7	3.6	3.0	6.0	4.1	20.9	6.0	4.4	3.7	6.5	3.8	3.5	5.9	5.8	5.9	2.0	11.0	4.3	2.3	6.1
Ba	487	713	610	1114	419	803.0	785	793	625	684	742	995	1024	664	661	669	784	803	732	897	696
La	30.6	37.5	30.3	22.4	28.7	23.3	57.9	31.6	41.2	41.3	30.9	50.8	44.1	26.9	31.6	25.4	28.5	45.2	42.9	20.4	35
Ce	61.5	75.8	62.0	47.2	60.1	44.3	114.1	60.0	82.4	86.4	61.6	104.5	97.2	58.1	63.1	51.7	59.2	91.1	86.5	41.7	71.5
Pr	7.2	9.4	7.5	5.6	7.2	7.4	13.7	7.2	9.4	10.5	7.3	12.4	11.3	6.6	7.7	6.1	6.8	10.5	10.1	4.9	8.9
Nd	26.8	35.5	27.9	21.2	27.1	27.9	52.0	29.4	34.6	40.7	27.6	48.2	40.8	25.3	28.5	23.5	25.6	38.8	37.6	17.7	33.3
Sm	5.3	8.2	6.3	5.1	6.6	6.5	11.3	5.9	6.6	8.5	5.6	9.5	8.5	5.4	6.0	5.3	5.2	8.6	7.7	4.2	6.9
Eu	1.1	1.0	0.8	1.0	0.7	0.9	1.5	1.6	1.3	1.4	1.4	1.4	1.5	1.1	1.2	1.1	1.3	1.1	1.1	1.2	1.3
Gd	4.4	7.3	6.0	4.7	6.6	6.1	9.7	4.6	5.3	7.0	4.9	8.5	7.6	4.5	5.8	5.0	4.8	7.3	6.6	3.9	6.0
Tb	0.7	1.2	1.1	0.8	1.2	1.1	1.6	0.7	0.8	1.1	0.8	1.3	1.1	0.7	0.9	0.7	0.8	1.1	1.1	0.7	0.9
Dy	4.4	8.2	6.6	4.9	7.9	6.9	9.5	4.1	5.1	6.0	5.1	7.8	6.3	4.4	5.2	4.4	5.2	6.4	6.5	3.9	5.6

Table 5 (Contd.)

Sample Lithotype	11X3a Orthogneisses	AP-16	AP 26	AP-15	AP 28	*Average*	H-373 Paragneisses	GFS415	H-163	S4-99	F17-2	FD36	FD47	GFS417	S2-00	S1-00	S1-99	S3-99	H-168	S2-99	*Average*
Area	Bados	Golfo Aranci				11 samples	Golfo Aranci														23 samples
Ho	0.9	1.6	1.3	1.0	1.6	1.4	1.8	0.8	1.0	1.2	1.0	1.5	1.1	0.8	1.0	0.9	1.0	1.3	1.4	0.8	1.1
Er	2.7	4.4	3.9	2.5	4.3	3.8	4.9	2.4	2.8	3.0	2.9	3.8	3.0	2.3	2.9	2.2	3.0	3.5	4.7	2.4	3.0
Tm	0.4	0.7	0.6	0.4	0.6	0.6	0.7	0.4	0.4	0.4	0.4	0.6	0.4	0.4	0.4	0.4	0.5	0.5	0.8	0.4	0.5
Yb	3.0	4.4	3.9	2.3	4.0	3.6	4.7	2.5	2.8	3.1	2.9	3.7	2.8	2.4	3.0	2.6	3.4	3.7	5.8	2.5	3.2
Lu	0.5	0.6	0.6	0.3	0.6	0.5	0.6	0.4	0.4	0.5	0.4	0.6	0.4	0.4	0.4	0.4	0.5	0.6	0.9	0.4	0.5
Hf	3.1	5.7	4.5	3.9	5.5	4.9	6.1	5.0	5.0	5.9	5.4	7.9	6.9	3.5	4.0	3.8	3.8	5.2	5.5	2.2	5.1
Ta	0.8	0.8	0.9	0.6	0.9	0.8	1.4	1.1	1.1	1.2	1.0	0.9	0.7	1.6	1.4	1.5	1.1	1.1	1.0	1.2	1.1
W	1.7	1.6	0.7	0.4	0.8	0.9	1.3	1.1	< DL	0.3	0.7	1.0	0.2	1.9	1.7	1.7	1.2	0.5	0.2	1.5	1.0
Pb	16.6	29.9	34.4	39.3	26.5	34.4	15.8	19.4	17.9	23.6	22.2	35.8	29.9	35.2	31.8	35.7	35.9	25.8	27.1	38.6	24.6
Bi	< DL	< DL	0.1	< DL	0.1	0.1	0.2	0.1	< DL	0.1	< DL	0.1	0.1	< DL	< DL	< DL	< DL	0.1	< DL	< DL	0.1
Th	9.7	16.4	12.8	8.0	14.0	14.5	15.8	7.2	10.6	17.9	8.5	21.9	17.7	9.8	11.5	9.6	10.4	22.9	15.0	6.7	13.1
U	2.1	3.6	2.8	1.7	3.4	3.6	4.8	2.0	1.8	3.6	2.4	4.1	1.8	3.8	5.9	8.7	2.4	4.2	3.3	3.3	3.7

The amphibolites and eclogites of northern Sardinia locally preserve bodies of ultramafic cumulates and layered amphibolite sequences (Franceschelli et al. 2005a and references therein). The metabasite chemical and isotopic composition spans from typical subalkaline N or T-MORB to continental tholeiite affinity (Franceschelli et al. 2005a; Giacomini et al. 2005). Often, field and chemical data point to derivation from intrusive protoliths (Ghezzo et al. 1979; Cruciani et al. 2002; Franceschelli et al. 2002, 2005a). Recent geochronological studies (Cortesogno et al. 2004; Palmeri et al. 2004; Giacomini et al. 2005) revealed that protolith ages concentrate between 460 and 450 Ma: metabasites are thus on average slightly younger than the felsic orthogneisses.

The minor mafic metavolcanic rocks associated with the felsic Ordovician volcano-sedimentary sequences in central and southern Sardinia have not been investigated in detail, but they are considered to be subalkaline (Memmi et al. 1982). Alkaline basalts with within-plate affinity occur in the nappe zones; but they represent younger events, being emplaced within the Devonian and Silurian sedimentary sequences (Ricci and Sabatini 1978; Di Pisa et al. 1992).

In conclusion, an Ordovician widespread magmatic activity is well attested in Sardinia both in the nappe zones and in the high-grade migmatitic zone. Crustal derived felsic metagranitoids and metavolcanics represent the dominant magmatic products. The occurrence of amphibolite and layered amphibolite sequences with tholeiite affinity in the high-grade basement points also to an important mantle contribution during Middle–Upper Ordovician times.

The Early Palaeozoic sedimentary sequence

The Variscan tectono-metamorphic overprint in the high-grade metamorphic basement that locally reached anatectic conditions and caused the profound textural resetting of metasedimentary rocks only partially affected zircons in these lithotypes. The majority of zircons in paragneisses preserve an older historical record, as demonstrated by in-situ U/Pb geochronology.

Middle Ordovician detrital zircons are the dominant population in migmatites: they have typical magmatic features, thus indicating a direct derivation from intrusive–effusive sequences of this age (480–450 Ma). The well-preserved shapes of many Ordovician zircons denote short transport and reworking during sedimentation. Therefore, as inferred from whole rock chemical and mineralogical compositions, the protoliths of the dated migmatites are young, immature shelf sediments representing the proximal erosion products of Ordovician magmatic rocks from adjoining areas.

Zircon isotope analyses indicate moreover that the metasediments sampled a basement containing significant igneous and metamorphic components related to

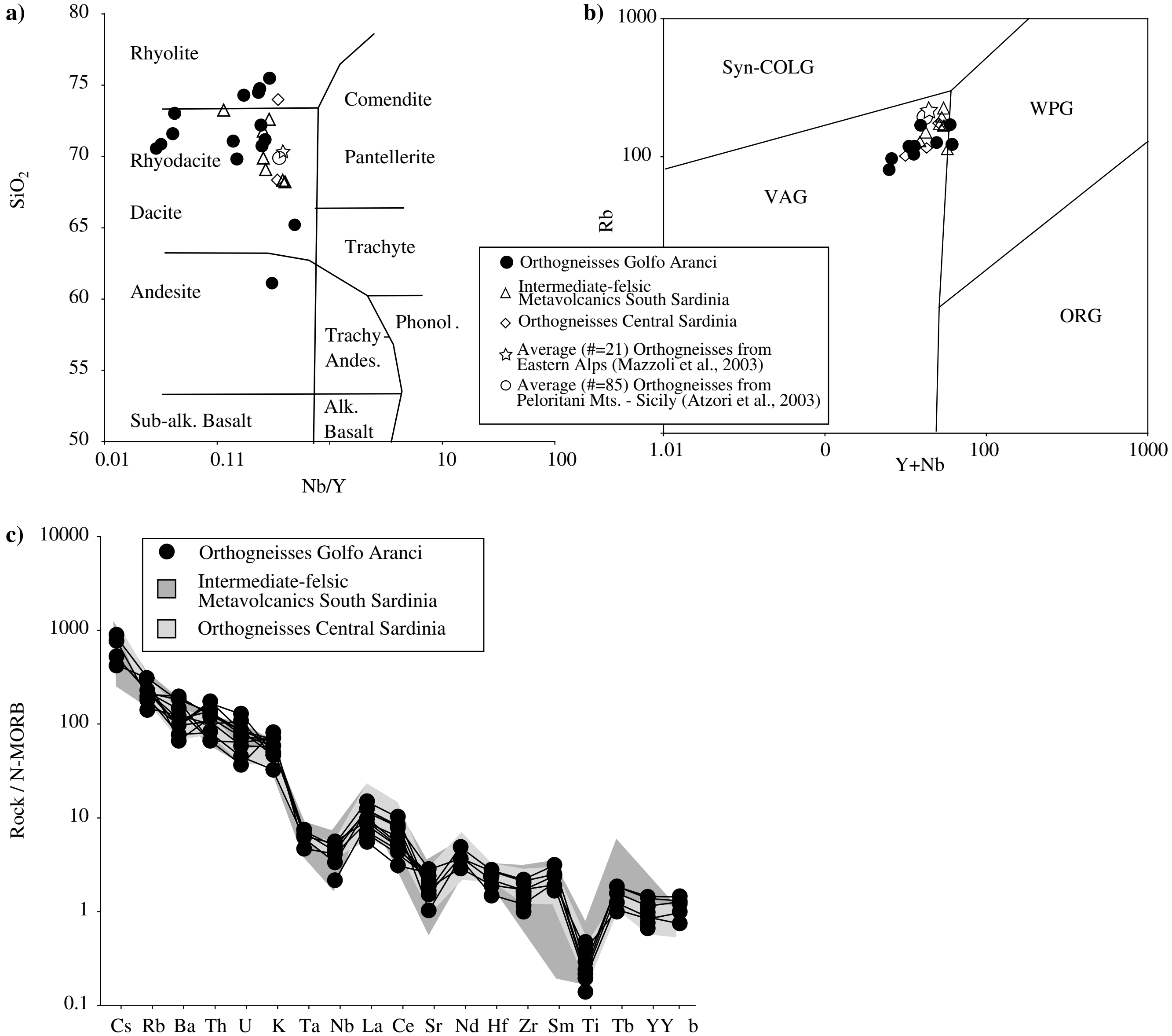

Fig. 6 Geochemical classification and WR trace element patterns of representative orthogneisses and metavolcanics from the Sardinian basement

the Cadomian orogenic cycle (550–650 Ma), up to now never clearly demonstrated in Corsica and Sardinia (Franceschelli et al. 2005b). The few inherited zircons older than 700 Ma concentrate between 800–1,200 and 1,700–2,300 Ma, with a possible age gap between 1,200 and 1,700 Ma; however, they are too few to precisely define the provenance and affinities of these very old sources.

We believe that the Middle Ordovician age of detrital zircons in the Sardinian migmatite represents a maximum depositional age for the sedimentary sequence (Fig. 8). Comparison with literature data (see Carmignani 2001 for a detailed review) suggests that the protoliths of the migmatites may correspond to the low-grade clastic sediments of central and southern Sardinia overlying or interlayered with the Ordovician metavolcanics. The undated metapelite–metamarl minor occurrences in the Golfo Aranci area could therefore be the high-grade counterpart of the Siluro-Devonian metasediments of central and southern Sardinia. These sediments testify the opening of a sedimentary basin deepening and expanding in the Late Ordovician–Silurian times.

Stratigraphic and geochronological data do not constrain the minimum depositional age of the sedimentary protoliths from the high-grade complex. There is only clear evidence of their involvement in the Variscan orogenic event at least from about 350 Ma (Ferrara et al. 1978; Di Vincenzo et al. 2004; Giacomini et al. 2005).

Fig. 7 Geochemical classification, inferred sources and depositional environment of representative metasediments from the high-grade Sardinia–Corsican basement. A: ocean island arc; B: continental island arc; C: active continental margin; D: passive continental margin

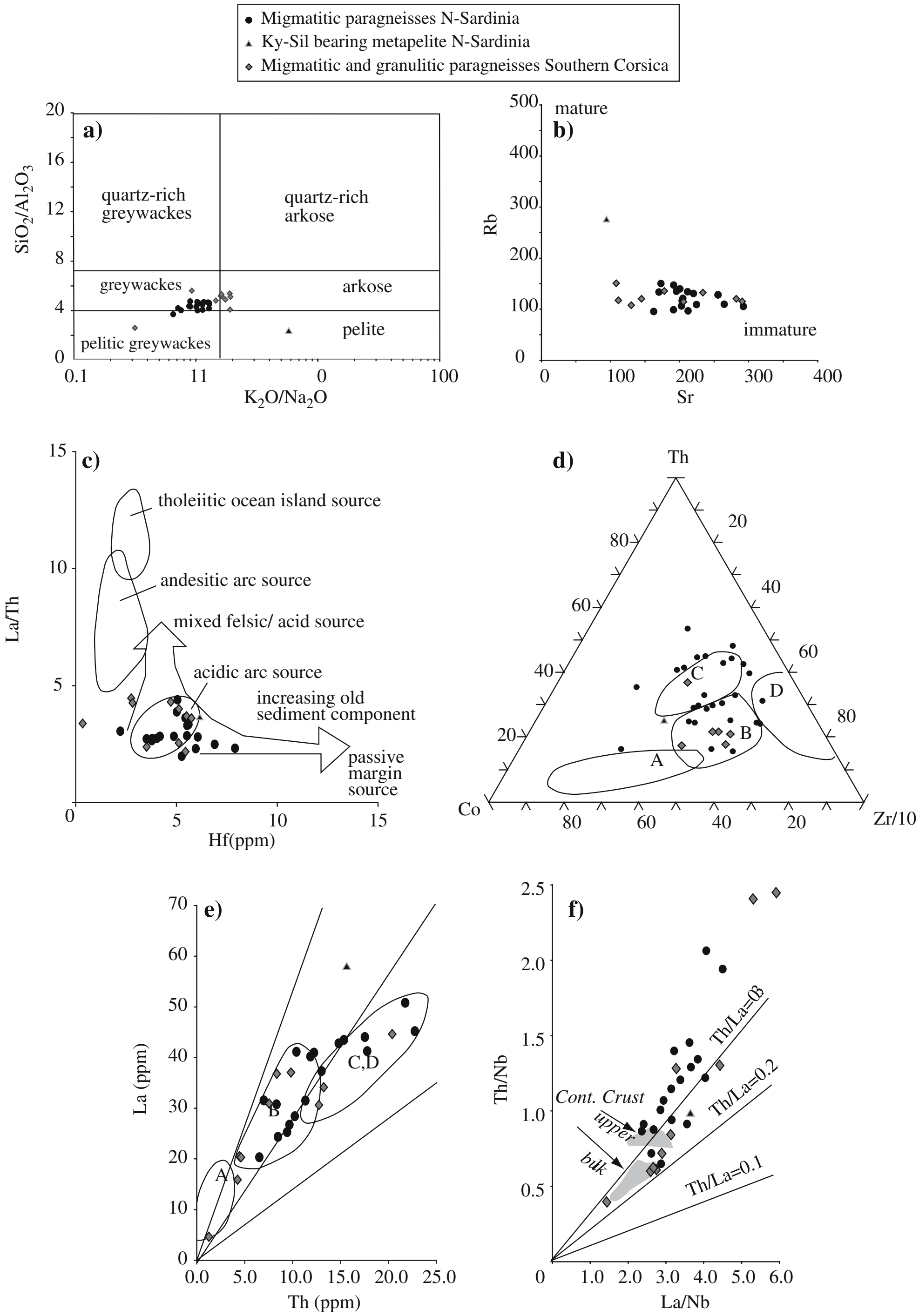

Variscan evolution

The lithostratigraphy and reconstructed metamorphic history of the Golfo Aranci area are similar to those of other high-grade outcrops in northern Sardinia (Carosi and Oggiano 2002; Carosi and Palmeri 2002; Ricci et al. 2004; Franceschelli et al. 2005b; Giacomini et al. 2005). The oldest metamorphic event recorded in the Golfo Aranci basement rocks is a still undated high-pressure eclogite-facies equilibration (~2.0 GPa/700°C) recorded by some metabasite outcrops. This event was followed by pervasive overprint under granulite to upper-amphibolite-facies conditions (1.3–0.9 GPa/750–800°C: Giacomini et al. 2005).

Although there is no evidence of high-pressure metamorphism in the felsic gneisses, the frequent interlayering of small eclogite boudins and stromatic migmatites suggests that these rocks were associated prior to metamorphic equilibration. The oldest relic textures and parageneses preserved within the felsic

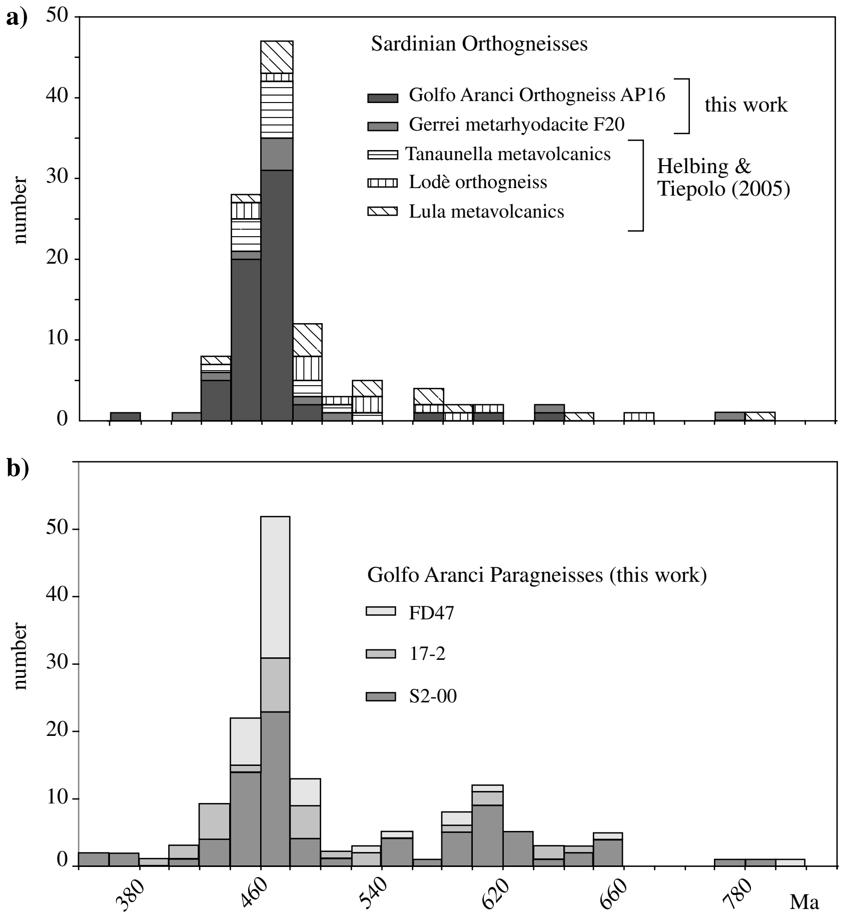

Fig. 8 **a** Cumulative histogram of U/Pb zircon ages from orthogneisses and metavolcanics of the Sardinian basement (data from this work and Helbing and Tiepolo 2005); **b** cumulative histogram of U/Pb zircon ages from the Sardinian metasediments analysed in this work

rocks (particularly within the metapelite sequences) point to equilibration under granulite to upper-amphibolite-facies conditions, with the formation of migmatites most likely due to the muscovite dehydration reaction:

$$Ms + Pl + Qtz = Kfs + Al_2SiO_5 + Melt.$$

The migmatisation event most likely started in the kyanite stability field at about 750–800°C and pressures above 1.0 GPa (see Giacomini et al. 2005 for more details); it may have continued into the sillimanite field due to nearly isothermal decompression.

Geochronological data suggest that metabasite and felsic gneisses shared the same PT evolution, at least since granulite-facies equilibration 350–330 Ma ago. The pervasive decompressional overprint and related zircon resetting 350 Ma ago in metabasic rocks (Giacomini et al. 2005) is interpreted as the result of fluid infiltration in the anhydrous mafic system during the migmatisation of the neighbouring metasediments. Moreover, the presence in migmatites of zircons with 350–320 Ma old metamorphic rims further sustains that the metamorphic equilibration is coeval in the mafic rocks and felsic gneisses.

The Variscan tectono-metamorphic evolution proceeded, during the exhumation stage, with pervasive deformation under a transpressive dextral shear regime (Carosi and Palmeri 2002). Deformation was associated with widespread heterogeneous retrograde mineralogical equilibration, which led to the development of lower-amphibolite-parageneses attested by the growth of retrograde white mica with Ar/Ar ages of 320–300 Ma (Di Vincenzo et al. 2004). Muscovite rims around kyanite and quartz–plagioclase myrmekite are further evidence of pervasive retrograde equilibration under amphibolite-facies conditions. The final stages of the Variscan orogenic cycle are marked by the widespread intrusion of syn- to posy-kinematic granites at shallow crustal levels about 310–290 Ma ago, producing the high-temperature–low-pressure metamorphic overprint along the intrusive contacts (Del Moro et al. 1975; Di Vincenzo et al. 1996).

Conclusions: a geodynamic scenario

Geochemical and geochronological analyses indicate that the felsic orthogneisses in the high-grade basement of Sardinia and Corsica are of Middle Ordovician age. Thus, they are the intrusive counterparts of the coeval metavolcanics from central and southern Sardinia. In addition, the metabasites with relic eclogite parageneses are not restricted to the Posada-Asinara mylonitic belt, but crop out extensively throughout the Sardinian high-grade basement (possibly up to northern Corsica, Palagi et al. 1985) and their protoliths are of Ordovician age (Cortesogno et al. 2004; Palmeri et al. 2004; Giacomini et al. 2005). The protoliths of the dominant migmatitic paragneisses in northern Sardinia and Corsica are siliciclastic shelf sediments (greywackes–arkoses) linked to the dismantling of the Ordovician magmatic belt. Therefore, we hypothesise that the high-grade metamorphic complex is not a fragment of the Precambrian Armorican basement as proposed by some authors (Cappelli et al. 1992; Carmignani 2001), but rather belongs to the same crustal segment of central-southern Sardinia representing a lateral basin sequence of the Ordovician volcano-sedimentary belt.

Taking also into account the post-Oligocene opening of the Liguro-Provençal basin, the counter-clockwise rotation of Sardinia–Corsica, the southeastern drifting of the Calabria and northern Sicily basements up to their actual position (Arthaud and Matte 1977; Speranza 1999; Faccenna et al. 2004), and the geological affinities among several Palaeozoic crustal sections in Italy, Provence and the Pyrenees (Paquette et al. 1989; von-Raumer et al. 1999; Barbey et al. 2001; Rubatto et al. 2001; Briand et al. 2002; Deloule et al. 2002; Atzori et al. 2003; Mazzoli et al. 2003; Friedl et al. 2004; Schulz et al. 2004; Trombetta et al. 2004), we propose a common geodynamic evolution for the entire area: the structure of this part of the southern Variscan belt derived from the tectonic stacking of the northern passive margin of an Ordovician–Silurian (-Devonian?) basin—the Palaeotethys as proposed by Stampfli et al. (2002)—along an active continental margin in the Devonian–Carboniferous. The high-grade metamorphic complex in northern Sardinia and Corsica thus corresponds to the main collisional zone characterised by maximum crustal thickening and subsequent maximum exhumation, whereas the nappe zone of southern Sardinia represents the back-arc fold and thrust belt.

This reconstruction is compatible with the models recently proposed for other sectors of the Variscan chain (Stampfli and Borel 2002; Stampfli et al. 2002; von Raumer et al. 2003; Drost et al. 2004; Mingram et al. 2004; Teipel et al. 2004; Zeck et al. 2004; Żelaźniewicz et al. 2004). Most authors agree that the Palaeozoic evolution started with a Cambro-Ordovician rift affecting the northern Gondwana margin (Figs. 9, 10). Following Linneman et al. (2000), Neubauer (2002) and von Raumer et al. (2003), between the Neoproterozoic and the Ordovician the northern margin of Gondwana underwent a series of collisions and fragmentations induced by Gondwana-verging oceanic subductions. After subduction of the Rheic ocean and amalgamation of Cadomia against Gondwana (Fig. 9b),

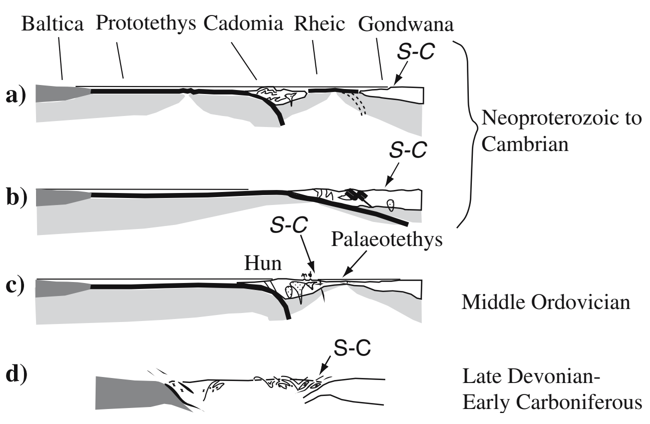

Fig. 9 Schematic geodynamic reconstruction of the Palaeozoic evolution at the northern Gondwana Margin; *Sard-Cor* indicates the inferred position of Sardinia and Corsica

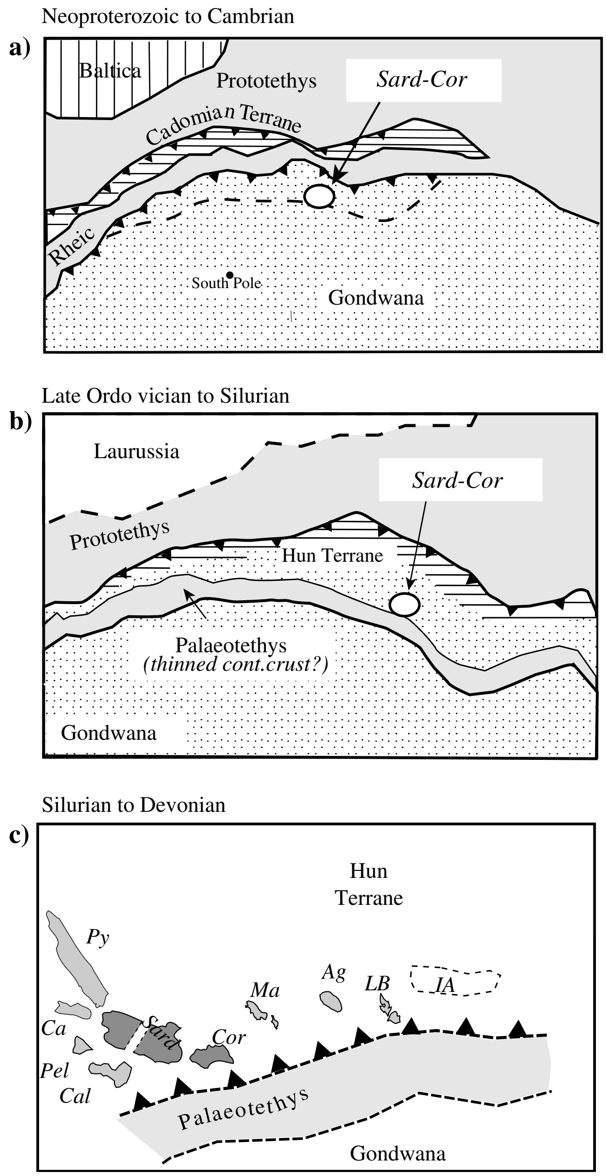

Fig. 10 Possible palaeogeographic reconstruction of the pre-Variscan plate arrangement at the northern Gondwana margin, see text for details (modified after: Linneman et al. 2000; Neubauer 2002; Vai 2001; von Raumer et al. 2003). *Sard*: Sardinia; *Cor*: Corsica; *Py*: Pyrenees; *Ca*: Catalan coastal range; *Ma*: Maures; *Pel*: Peloritani (Sicily); *Cal*: Calabria; *Ag*: Argentera; *LB*: Ligurian Briançonnais; *IA*: other intra-alpine massifs

a composite block of terranes affected by the cordillera-type magmatism (the Hun Terranes) started to evolve towards an arc setting (Fig. 9c) and to detach from Gondwana in response to the south-verging subduction of the Prototethys ocean (separating Gondwana from Laurussia). Whether the Palaeotethys break-up actually evolved into an oceanic domain is uncertain. Nevertheless, the subsequent northward drifting of Gondwana and the subduction of this new extensional basin—probably a thinned continental crust (Vai 2001)—under the Hun Terranes marked the inception of the Variscan orogenic cycle in southern Europe (Figs. 9d, 10c). In this context, the still undated high-pressure metamorphism recorded by the Sardinian metabasites confirms the presence of a subduction environment under the Sardinia–Corsica microplate, which belonged entirely to the Hun Terranes. The ensuing widespread granulite/upper-amphibolite-facies metamorphism in the Carboniferous testifies to the continental collision between the Gondwanan plate and its derived northern terranes.

Acknowledgements Zircon dating and trace element analyses could not have been possible without the valuable collaboration of Bill Griffin (GEMOC Key Centre, Macquarie University, Sydney) and Massimo Tiepolo (CNR-Istituto di Geoscienze e Georisorse of Pavia, Italy). Thanks are due to Giuliana de Grandis (CNR-IGG of Pisa) for assistance during zircon separation. This manuscript has been substantially improved by the reviews of Gaston Godard and Juergen von Raumer: both are kindly acknowledged.

References

Andersen T (2002) Correction of common lead in U–Pb analyses that do not report ^{204}Pb. Chem Geol 192:59–79

Andersen T, Griffin WL (2004) Lu–Hf and U–Pb isotope systematics of zircons from the Storgangen intrusion, Rogaland Intrusive Complex, SW Norway: implications for the composition and evolution of Precambrian lower crust in the Baltic Shield. Lithos 73:271–288

Andersen T, Griffin WL, Pearson NJ (2002) Crustal evolution in the SW part of the Baltic Shield: the Hf isotope evidence. J Petrol 43:1725–1747

Arthaud F, Matte P (1977) Détermination de la position initiale de la Corse et de la Sardaigne à la fin de l'orogenèse hercynienne grâce aux marqueurs géologiques anté-mésozoïques. Bull Soc Géol Fr 19(4):833–840

Atzori P, Cirrincione R, Kern H, Mazzoleni P, Pezzino A, Puglisi G, Punturo R, Trombetta A (2003) The abundance of 55 elements and petrovolumetric models of the crust in the NE Peloritani mountains. In: Sassi FP (ed) The abundance of 55 elements and petrovolumetric models of the crust in 9 type areas from the crystalline basement of Italy, with some geophysical and petrophysical data. Accademia Nazionale dei Lincei, Roma

Barbey P, Cheilletz A, Laumonier B (2001) The Canigou orthogneisses (Eastern Pyrenees, France, Spain): an Early Ordovician rapakivi granite laccolith and its contact aureole. C R Acad Sci Paris Série II 332(2):129–136

Bard JP (1997) Démembrement anté-mesozoïque de la chaîne varisque d'europe occidentale et d'Afrique du Nord: rôle essentiel des grands décrochements transpressifs dextres accompagnant la rotation–translation horaire d'Afrique durant le Stéphanien. C R Acad Sci Paris, 324, Série IIa, 693–704

Bathia MR (1983) Plate tectonics and geochemical composition of sandstones. J Geol 91:611–627

Bathia MR, Crook KAW (1986) Trace elements characteristics of greywackes and mudrocks: provenance and tectonic setting interpretation. Sediment Geol 41:249–268

Bodet F, Schärer U (2000) Evolution of the SE-Asian continent from U–Pb and Hf isotopes in single grains of zircon and baddeleyite from large rivers. Geochim Cosmochim Acta 64:2067–2092

Briand B, Bouchardon JL, Capiez P, Piboule M (2002) Felsic (A-type) -basic (plume-induced) Early Palaeozoic bimodal magmatism in the Maures Massif (southeastern France). Geological Magazine 139(3):291–311

Cappelli B, Carmignani L, Castorina F, Di Pisa A, Oggiano G, Petrini R (1992) A Hercynian suture zone in Sardinia: geological and geochemical evidence. Geodin Acta 5(1–2):101–118

Carmignani L (2001) Geologia della Sardegna. Memorie descrittive della Carta Geologica d'Italia, vol LX. Servizio Geologico d'Italia, Roma

Carmignani L, Rossi P (2001) Carta Geologica e Strutturale della Sardegna e della Corsica. In: Carmignani et al. (ed) Geologia della Sardegna. Memorie descrittive della Carta Geologica d'Italia, vol LX. Servizio Geologico d'Italia, Roma

Carmignani L, Barca S, Cappelli B, Di Pisa A, Gattiglio M, Oggiano G, Pertusati PC (1992) A tentative Geodynamic model for the Hercynian basement of Sardinia. In: Carmignani L, Sassi FP (eds) Contributions to the Geology of Italy with special regard to the Palaeozoic basements. IGCP 276-Newsletter 5, Siena, pp 61–83

Carmignani L, Carosi R, Di Pisa A, Gattiglio M, Musumeci G, Oggiano G, Pertusati PC (1994) The Hercynian chain in Sardinia (Italy). Geodin Acta 7(1):31–47

Carosi R, Oggiano G (2002) Transpressional deformation in northwestern Sardinia (Italy): insights on the tectonic evolution of the Variscan belt. C R Acad Sci Paris Série II 334:287–294

Carosi R, Palmeri R (2002) Orogen-parallel tectonic transport in the Variscan belt of northeastern Sardinia (Italy) : implications for the exhumation of medium-pressure metamorphic rocks. Geol Mag 139(5):497–511

Compston W, Williams IS, Kirschvink JL, Zhang Z, Ma C (1992) Zircon U–Pb ages for the Early Cambrian time-scale. J Geol Soc London 149:171–184

Cortesogno L, Gaggero L, Oggiano G, Paquette JL (2004) Different tectono-thermal evolutionary paths in eclogitic rocks from the axial zone of the Variscan Chain in Sardinia (Italy) compared with the Ligurian Alps. Ofioliti 29(2):125–144

Cruciani G, Franceschelli M, Marchi M, Zucca M (2002) Geochemistry of metabasites from NE Sardinia, Italy: nature of the protoliths, magmatic trend and geotectonic setting. Mineral Petrol 74:25–47

Cruciani G, Franceschelli M, Caredda AM, Elter FM (2003) Metamorphic evolution of Variscan migmatites in NE Sardinia. J Czech Geol soc 48(1–2):36–37

Del Moro A, Si Simplicio P, Ghezzo C, Guasparri G, Rita F, Sabatini G (1975) Radiometric data and intrusive sequence in the Sardinian Batholith. N Jb Miner Abh 126:28–44

Delaperrière E, Lancelot J (1989) Datation U–Pb sur zircons de l'orthognéiss du Capo Spartivento (Sardaigne, Italie), nouveau témoin d'un magmatisme alcalin Ordovicien dans le Sud de l'Europe. C R Acad Sci Paris Série II 309:835–842

Deloule E, Alexandrov P, Cheilletz A, Laumonier B, Barbey P (2002) In-situ U–Pb zircon ages for Early-Ordovician magmatism in the eastern Pyrenees, France: the Canigou orthogneisses. Int J Earth Sci 91:398–405

Di Pisa A, Gattiglio M, Oggiano G (1992) Pre-Hercynian magmatic activity in the Nappe Zone (Internal and External) of Sardinia: evidence of two within plate basaltic cycles. In: Carmignani L, Sassi FP (eds) Contributions to the Geology of Italy with special regard to the Palaeozoic basements. IGCP 276-Newsletter 5, Siena

Di Simplicio P, Ferrara G, Ghezzo C, Guasparri G, Pellizzer R, Ricci CA, Rita F, Sabatini G (1974) Il metamorfismo e il magmatismo paleozoico della Sardegna. Rendiconti Società Italiana Mineralogia e Petrografia 30:979–1068

Di Vincenzo GF, Andriessen PAM, Ghezzo C (1996) Evidence of two different components in a Hercynan peraluminous cordierite-bearing granite: the San Basilio intrusion (central Sardinia, Italy). J Petrol 37(5):1175–1206

Di Vincenzo G, Carosi R, Palmeri R (2004) The relationship between tectono-metamorphic evolution and argon isotope records in white micas: constraints from in situ 40Ar–39Ar laser analysis of the Variscan basement of Sardinia (Italy). J Petrol 45(1013–1043)

Drost K, Linneman U, McNaughton N, Fatka O, Kraft P, Gehmlich M, Tonk C, Marek J (2004) New data on the Neoproterozoic—Cambrian geotectonic setting of the Tépla-Barrandian volcano-sedimentary successions: geochemistry, U–Pb zircon ages and provenance (Bohemian Massif, Czech Republic). Int J Earth Sci 93(5):742–757

Edel JB (2000) Hypothèse d'une ample rotation horaire tardivarisque du bloc Maures-Estérel-Corse-Sardaigne. Géologie de la France 1:3–19

Elter FM, Ghezzo C (1995) La "Golfo Aranci shear zone" (Sardegna NE): una zona di taglio polifasica tardo ercinica. Boll Soc Geol Ital 114:147–154

Elter FM, Palmeri R (1992) The Calc-silicate marble of Tamarispa (NE Sardinia). In: Carmignani L, Sassi FP (eds) Contributions to the geology of Italy with special regards to the Palaeozoic basements. IGCP N°276, NEWSLETTER 5:117–121

Faccenna C, Piromallo C, Crespo-Blanc A, Jolivet L, Rossetti F (2004) Lateral slab deformation and the origin of the western Mediterranean arcs. Tectonics 23:1–21

Ferrara G, Rita F, Ricci CA (1978) Isotopic age and tectono-metamorphic history of the metamorphic basement of North-eastern Sardinia. Contrib Mineral Petrol 68(99–106)

Floyd PA, Leveridge BE (1987) Tectonic environment of the Devonian Gramscatho basin, South Cornwall: Framework mode and geochemical evidence from turbiditic sandstones. J Geol Soc London 144:531–542

Franceschelli M, Carcangiu G, Caredda AM, Cruciani G, Memmi I, Zucca M (2002) Tranformation of cumulate mafic rocks to granulite and re-equilibration in amphibolite and greenschist facies in NE Sardinia, Italy. Lithos 63:1–18

Franceschelli M, Puxeddu M, Cruciani G, Dini A, Loi M (2005a) Layered amphibolite sequence in NE Sardinia, Italy: remnant of a pre-Variscan mafic silicic layered intrusion? Contrib Mineral Petrol 149(2):164–180

Franceschelli M, Puxeddu M, Cruciani G (2005b) Variscan metamorphism in Sardinia, Italy: review and discussion. In: Carosi R, Dias R, Iacopini D, Rosenbaum G (eds) The southern Variscan belt. J Virtual Explor, Electronic Edition, ISSN 1441–8142, 19

Franke W (2000) The mid-European segment of the Variscides: tectonostratigraphic units, terrane boundariesand plate tectonic evolution. In: Franke W, Haak V, Oncken O, Tanner D (eds) Orogenic processes: quantification and modelling of the Variscan Belt. Geological society of London, Special Publications 179, London, pp 35–61

Friedl G, Finger F, Paquette JL, von Quadt A, McNaughton NJ, Fletcher IR (2004) Pre-Variscan geological events in the Austrian part of the Bohemian Massif deduced from U–Pb zircon ages. Int J Earth Sci 93(5):802–823

Garbarino C, Naitzla S, Rizzo R, Tocco S, Barca S, Farci A, Serri R (2005) New evidence of pre-Hercynian volcanics from Southern Sulcis (Southwestern Sardinia). Boll Soc Geol Ital 124:69–85

Ghezzo C, Memmi I, Ricci CA (1979) Un evento granulitico nel basamento metamorfico della Sardegna nord-orientale. Memorie della Società Geologica Italiana 20:23–38

Giacomini F, Bomparola RM, Ghezzo C (2005) Petrology and geochronology of metabasites with eclogite facies relics from NE Sardinia: constraints for the Palaeozoic evolution of Southern Europe. Lithos 82:221–248

Griffin WL, Pearson NJ, Belousova EA, Jackson SE, van Achterbergh E, O'Reilly SY, Shee SR (2000) The Hf isotope composition of cratonic mantle: LAM-MC-ICPMS analysis of zircon megacrysts in kimberlites. Geochim Cosmochim Acta 64:133–147

Hanchar JM, Miller CF (1993) Zircon zonation patterns as revealed by cathodoluminescence and back-scattered electron images: implications for interpretation of complex crustal histories. Chem Geol 110:1–13

Helbing H (2003) No suture zone in the Sardinian Variscides: a structural, petrological and geochronological analysis. Tueb Geowiss Arb. A68, (ISSN 0953–4921), 190 pp

Helbing H, Tiepolo M (2005) Age determination of Ordovician magmatism in NE Sardinia and its bearing on Variscan basement evolution. J Geol Soc London 162:1–12

Hinton RW, Upton BGJ (1991) The chemistry of zircon: variations within and between large crystals from syenite and alkali basalt xenoliths. Geochim Cosmochim Acta 55:3287–3302

Hoskin PWO, Black LP (2000) Metamorphic zircon formation by solid-state recrystallization of protolith igneous zircon. J Metamorph Geol 18(4):423–439

Linnemann U, Gehmlich M, Tichomirova M, Buschmann B, Nasdala L, Jonas P, Lützner H, Bombach K (2000) From Cadomian subduction to Early Palaeozoic rifting: the evolution of Saxo-Thuringia at the margin of gondwana in the light of single zircon geochronology and basin development (Central European Variscides, Germany). In: Franke W (ed) Orogenic processes: quantification and modelling in the Variscan Belt. Geol Soc London

Ludwig KR, Turi B (1989) Paleozoic age of the Capo Spartivento Orthogneiss, Sardinia, Italy. Chem Geol 79:147–153

Matte P (1986) Tectonics and plate tectonics model for the Variscan belt of Europe. Tectonophysics 196:309–339

Matte P (1998) HP rocks in Palaeozoic orogenic belt: uralides and variscides., tectonics and general history of phanerozoic orogens. J Geol Soc Schweden, pp 209–222

Matte P (2001) The Variscan collage and orogeny (480–290 Ma) and the tectonic definition of the Armorica microplate. Terra Nova 13(2):122–128

Mazzoli C, Sassi R, Burlini L, Cesare B, Peruzzo L, Spiess R, Sassi FP (2003) The abundance of 55 elements and petrovolumetric models of the crust in the Aurina and Pusteria Valleys. In: Sassi FP (ed) The abundance of 55 elements and petrovolumetric models of the crust in 9 type areas from the crystalline basement of Italy, with some geophysical and petrophysical data. Accademia Nazionale dei Lincei, Roma

Memmi I, Barca S, Carmignani L, Cocozza T, Elter FM, Franceschelli M, Gattiglio M, Ghezzo C, Minzoni M, Naud G, Pertusati PC, Ricci CA (1982) Further geochemical data on the pre-Hercynian igneous activities of Sardinia and their geodynamic significance. In: Italiana MdSG (ed) Guida alla Geologia del Paleozoico Sardo. Guide Geologiche Regionali, pp 157–164

Menot RP, Orsini JB (1990) Evolution du socle anté-stéphanien de Corse: événements magmatiques et métamorphiques. Schweiz Miner Petrol Mitt 70:35–53

Miller L, Sassi FP, Armari G (1976) On the occurrence of altered eclogitic rocks in north-eastern Sardinia and their implications. N Jb Geol Paleont 11:683–689

Mingram B, Kröner A, Hegner E, Krentz O (2004) Zircon ages, geochemistry, and Nd isotopic systematics of pre-Variscan orthogneisses from the Erzgebirge, Saxony (Germany), and geodynamic interpretation. Int J Earth Sci 93(5):706–727

Neubauer F (2002) Evolution of late Neoproterozoic to early Paleozoic tectonic elements in Central and Southeast European Alpine mountain belts: review and synthesis. Tectonophysics 352:87–103

Palagi P, Laporte D, Lardeaux JM, Menot RP, Orsini JB (1985) Identification d'un complete leptyno-amphibolique au sein des "gneiss de Belgodère" (Corse occidentale). C R Acad Sci Paris Série II 301(14):1047–1052

Palmeri R (1992) Petrography and Geochemistry of some migmatites from Northeastern Sardinia (Italy). In: Carmignani L, Sassi FP (eds) Contributions to the geology of Italy with special regards to the Palaeozoic basements. IGCP N°276, NEWSLETTER 5:183–186

Palmeri R, Fanning M, Franceschelli M, Memmi I, Ricci CA (2004) SHRIMP dating of zircons in eclogite from the Variscan basement in north-eastern Sardinia (Italy). N Jb Miner Abh 6:275–288

Paquette JL, Menot RP, Peucat JJ (1989) REE, Sm–Nd and U–Pb zircon study of eclogites from the Alpine External Massifs (Western Alps): evidence for crustal contamination. Earth Planet Sci Lett 96:181–198

Pearce JA, Harris NBW, Tindle AG (1984) Trace element discrimination diagrams for the tectonic interpretation of granitic rocks. J Petrol 25:956–983

Plank T (2005) Constraints from thorium/lanthanum on sediment recycling at subduction zones and the evolution of the continents. J Petrol 46(5):921–944

Ricci CA (1992) From crustal thickening to exhumation: petrological, structural and geochronological records in the crystalline basement of northern Sardinia. In: Carmignani L, Sassi FP (eds) Contributions to the Geology of Italy with special regard to the Palaeozoic basements. IGCP 276-Newsletter 5, Siena, pp 187–197

Ricci CA, Sabatini G (1978) Petrogenetic affinity and geodynamic significance of metabasic rocks from Sardinia, Corsica and Provence. N Jb Miner Mh 1:23–38

Ricci CA, Carosi R, Di Vincenzo G, Franceschelli M, Palmeri R (2004) Unravelling the tectono-metamorphic evolution of medium-pressure rocks from collision to exhumation of the Variscan basement of NE Sardinia (Italy): a review. Period Miner 73(2):73–83

Rubatto D, Schaltegger U, Lombardo B, Colombo F, Compagnoni R (2001) Paleozoic magmatic and metamorphic evolution of the Argentera Massif (Western Alps) resolved with U–Pb dating. Schweiz Miner Petrol Mitt 81(2):213–228

Schulz B, Bombach K, Pawlig S, Brätz H (2004) Neoproterozoic to Early-Palaeozoic magmatic evolution in the Gondwana-derived Austroalpine basement to the south of the Tauern Window (Eastern Alps). Int J Earth Sci 93(5):824–843

Speranza F (1999) Paleomagnetism and the Corsica-Sardinia rotation: a short review. Bull Soc Geol Ital 118:1–7

Stampfli GM, Borel GD (2002) A plate tectonic model for the Paleozoic and Mesozoic constrained by dynamic plate boundaries and restored synthetic oceanic isochrons. EPSL 196:17–33

Stampfli GM, von Raumer J, Borel G (2002) The Palaeozoic evolution of pre-Variscan terranes: from Gondwana to the Variscan collision. In: Martinez Catalan JR, Hatcher RD, Arenas R, Diaz Garcia F (eds) Variscan-Appalacchian dynamics: the building of late Palaeozoic basement. GSA Special Paper 364:263–280

Teipel U, Eichhorn R, Loth G, Rohrmüller J, Höll R, Kennedy A (2004) U–Pb SHRIMP and Nd isotopic data from the western Bohemian Massif (Bayerischer Wald, Germany): implications for Upper Vendian and Lower Ordovician magmatism. Int J Earth Sci 93(5):782–801

Trombetta A, Cirrincione R, Corfu F, Mazzoleni P, Pezzino A (2004) Mid-Ordovician U–Pb ages of porphyroids in the Peloritan Mountains (NE Sicily): palaeogeographical implications for the evolution of the Alboran microplate. J Geol Soc London 161(2):265–276

Vai GB (2001) Basement and early (pre-Alpine) history. In: Vai, Martini (eds) Anatomy of an Orogen—the Apennines and adjacent Mediterranean Basins. Kluwer, Dordrecht

Vervoort JD, Patchett PJ (1996) Behavior of hafnium and neodymium isotopes in the crust: constraints from Precambrian crustally derived granites. Geochim Cosmochim Acta 60:3717–3723

von-Raumer J et al (1999) The Palaeozoic metamorphic evolution of the Alpine External Massifs. Schweiz Miner Petrol Mitt 79:5–22

von-Raumer J, Stampfli GM, Bussy F (2003) Gondwana derived microcontinents—the constitutents of the Variscan and Alpine collisional orogens. Tectonophysics 365:7–22

Wimmenauer W (1984) Das praevariszische Kristallin im Schwarzwald. Forscht Miner Beih 62:69–86

Zeck HP, Wingate MTD, Pooley GD, Ugidos JM (2004) A sequence of Pan-African and Hercynian events recorded in zircons from an orthogneiss from the Hercynian belt of Western Central Iberia—an ion microprobe U–Pb study. J Petrol 45(8):1613–1629

Żelaźniewicz A, Dörr W, Bylina P, Franke W, Haack U, Heinisch H, Schastok J, Grandmontagne K, Kulicki C (2004) The eastern continuation of the Cadomian orogen: U–Pb zircon evidence from Saxo-Thuringian granitoids in south-western Poland and the northern Czech Republic. Int J Earth Sci 93(5):773–781